GEORGIA INSTITUTE OF TECHNOLOGY
Engineering Experiment Station

PROJECT INITIATION

Date: October 25, 1973

Project Title: Assistance in a Study Program Related to Development of a Man-Worn Laser Detection Device.

Project No.: A-1567

Project Director: Mr. R. G. Shackelford

Sponsor: Electromagnetic Sciences, Inc., Norcross, Georgia 30071

Effective . . . September 17, 1973 . . . . . Estimated to run until: . December 21, 1973. . . . . .

Type Agreement: Contract No. SC-1730-091773 (Subcontract under Prime No. N61339-74-C-0021). . . . Amount: $ . . 37,517.00 . . . . . .

REPORTS REQUIRED: Preliminary Report; Final Report.

SPONSOR CONTACT PERSONS: Mr. William Baker
Vice-President, Marketing-Electronics
Electromagnetic Sciences, Inc.
P.O. Box 80508 - Chamblee
Atlanta, Georgia 30341

Phone: 448-5770

Assigned to Special Techniques & Sensor Systems . . . . Division ~~Division~~

COPIES TO:

Project Director	Photographic Laboratory
Director	Security, Property, Reports Coordinator
Assistant Director	EES Accounting
GTRI	EES Supply Services
Division Chief(s)	Library
Service Groups	Rich Electronic Computer Center
Patent Coordinator	Project File
	Other ~~R. M. Goodman~~

RA-62

GEORGIA INSTITUTE OF TECHNOLOGY
Engineering Experiment Station

PROJECT TERMINATION

Date February 4, 1974

PROJECT TITLE: "Assistance in a Study Program Related to Development of a Man-Worn Laser Detection Device"

PROJECT NO: A-1567

PROJECT DIRECTOR: Mr. R. G. Shackelford

SPONSOR: Electromagnetic Sciences, Inc., Norcross, Georgia 30071

TERMINATION EFFECTIVE: December 21, 1973 (Contract expiration)

CHARGES SHOULD CLEAR ACCOUNTING BY: N/A - all funds expended by 12-31-73.

CONTRACT CLOSEOUT ITEMS REMAINING: Final Invoice & Closing Documents
Final Report of Inventions
Government Property Inventory and/or Cert.

SPECIAL TECHNIQUES & SENSOR SYSTEMS DIVISIONS

COPIES TO:

Project Director
Director
Associate Director
Assistant Directors
Division Chief
Branch Head
Accounting
Engineering Design Services
General Office Services
Photographic Laboratory
Purchasing
Report Section
Library
✓Security
Rich Electronic Computer Center

R. M. Goodman, Jr.

ENGINEERING EXPERIMENT STATION
Georgia Institute of Technology
Atlanta, Georgia 30332

FINAL REPORT

PROJECT NO. A-1567

A STUDY PROGRAM RELATED TO THE DEVELOPMENT OF A MAN-WORN LASER DETECTION DEVICE

Subcontract under
Prime No. N61339-74-C-0021

By

R. G. Shackelford, J. M. Akridge and
A. McSweeney

RESEARCH CONTRACT SC-1730-091773

17 September 1973 to 21 December 1973

Performed for

ELECTROMAGNETIC SCIENCES, INC.
Norcross, Georgia 30071

ENGINEERING EXPERIMENT STATION
Georgia Institute of Technology
Atlanta, Georgia 30332

FINAL REPORT

PROJECT NO. A-1567

A STUDY PROGRAM RELATED TO THE DEVELOPMENT OF A MAN-WORN LASER DETECTION DEVICE

Subcontract under
Prime No. N61339-74-C-0021

By

R. G. Shackelford, J. M. Akridge and
A. McSweeney

RESEARCH CONTRACT SC-1730-091773

17 September 1973 to 21 December 1973

Performed for

ELECTROMAGNETIC SCIENCES, INC.
Norcross, Georgia 30071

ABSTRACT

This report describes the design, testing and development of a fiber optic array detector suitable for use as a man-worn detector of infrared radiation simulating small arms weapon fire. The design concept, which was developed on internal funding at the Engineering Experiment Station (EES) at Georgia Tech, consists of an array of fiber optic waveguides terminating normally into a cloth panel. The optical fibers were routed along the panel and collected in a single bundle which was terminated at the surface of a photodetector. Radiation coupled into the ends of the optical fibers at the surface of the panel was thus transmitted to the photodetector and its associated electronics where suitable processing was applied to detect properly coded pulses representing small arms weapon fire.

Field tests conducted by EMS, Inc. demonstrated that a system employing the end-coupled fiber optic detector panel and a GaAs laser illuminator resulted in a signal-to-noise ratio of 15 dB over a range of 25 to 300 meters with the laser illuminator operating at an intensity level which was about 7 dB below the maximum permissible eye-safe radiation level. Based on the results of these tests, an eye-safe small arms training system employing the fiber optic detector panel would provide a 22 dB signal-to-noise ratio over an engagement range of 25 to 300 meters.

TABLE OF CONTENTS

LIST OF FIGURES

LIST OF FIGURES (Continued)

LIST OF FIGURES (Continued)

LIST OF TABLES

1. INTRODUCTION

Over the past two and one-half years, the Engineering Experiment Station (EES) at Georgia Tech has engaged in an internally funded study and hardware implementation relating to the realization of a fiber optic array detector suitable for use in a Laser Engagement System of the type described in Reference [1]. These efforts are documented in two proposals from EES to EMS [2,3], and in a letter [4] which reviews the pursuit of a patent by EES on the fiber optic detector panel concept.

These preliminary efforts, along with the design and development of the electronic portion of the detector system and extensive field testing, both of which were performed by EMS, Inc., have led to a contract between the Naval Training Equipment Center and EMS for the development and delivery of a Man-Worn Laser Detector Device based on the fiber optic array detector developed earlier at EES. The work described in this report was performed by EES under contract with EMS to assist in the development of the man-worn detector system.

A fiber optic detector panel consisting of an array of 192 end-coupled optical fibers has been fabricated and delivered to EMS. The detector's optical performance has been measured, and the results of these measurements, along with field measurements performed at EMS, have been used to predict the performance of a man-worn training system employing the fiber-optic array detector and an eye-safe GaAs laser illuminator.

This report also contains the documented results of characteristic measurements performed on plastic fiber optics and other materials such as transparent tapes and encapsulents which were employed in the fabrication of the detector panel. The instrumentation used to perform these measurements was carefully calibrated at the wavelength of the GaAs laser diode illuminator.

In addition to the development of the end-coupled fiber optic array detector, tests were also performed on a small sample of a side-coupled fiber-optic configuration consisting of a woven panel of optical fibers

and cotton fibers. The results of optical coupling measurements on this sample and an estimate of its performance, as compared with the end-coupled array, are also presented.

Although several new approaches for implanting the optical fibers in the panel were tried during the course of this program, it should be noted that the final panel design, which exhibited excellent performance in the field, was virtually identical to the design concept generated in the in-house study described above [1,2,3].

2. CALIBRATION OF TEST INSTRUMENTATION

2.1 Spectral Profile of the GaAs Laser Diode

The power spectrum of the diode laser employed in the lab tests was measured with a Jarrell-Ash spectrometer, as shown in Figure 2.1. The purpose of this measurement was to insure spectral compatibility between the laser diode and the narrow band background elimination filter and to provide data for analysis of the transmission characteristics of the optical fibers. A lens was used to focus the pulsed laser radiation on the entrance slit of the spectrometer. The $1cm^2$ UDT optometer detector collected the radiation diffracted by the grating in the spectrometer. The output of the optometer was recorded while the grating was rotated to produce a graph of the power spectrum.

The measured power spectrum of the Laser Diode Laboratories LD 65 laser is shown in Figure 2.2. The center wavelength was 0.9055 μm and the Full Width at Half Maximum (FWHM) was 0.0025 μm. The manufacturer's specifications indicate a center wavelength of 0.905 μm and a FWHM of 0.0025 μm, so the measured values are in agreement with the expected values.

2.2 Pulse Characteristics of GaAs Laser Diode

Several pulse circuits for driving diode lasers were assembled, tested, and modified for laboratory testing. In each case, the characteristics of the electrical driving pulses and of the radiation pulses were measured and compared on a dual trace oscilloscope as shown in Figure 2.3. A signal proportional to the current through the laser was developed across the series resistor and displayed on one channel of the oscilloscope. The pulsed laser radiation was detected by a small PIN photodiode and the signal was amplified and displayed on the second channel of the oscilloscope.

A pulse circuit based on a delay line was assembled and is shown in Figure 2.4. This device was made to be modified and used in the lab, so the components were mounted in such a way as to be easily accessible. The diode laser is in the foreground, almost directly above the mounting rod.

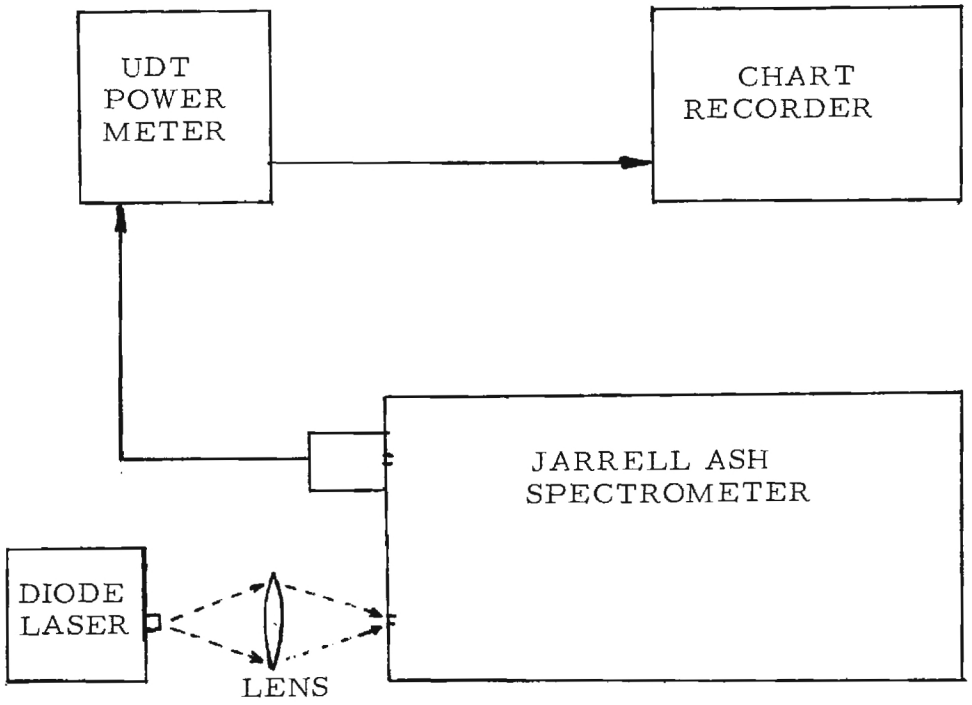

Figure 2.1. Block Diagram of the Experimental Setup Used to Measure the Spectral Characteristics of the GaAs Laser Diode.

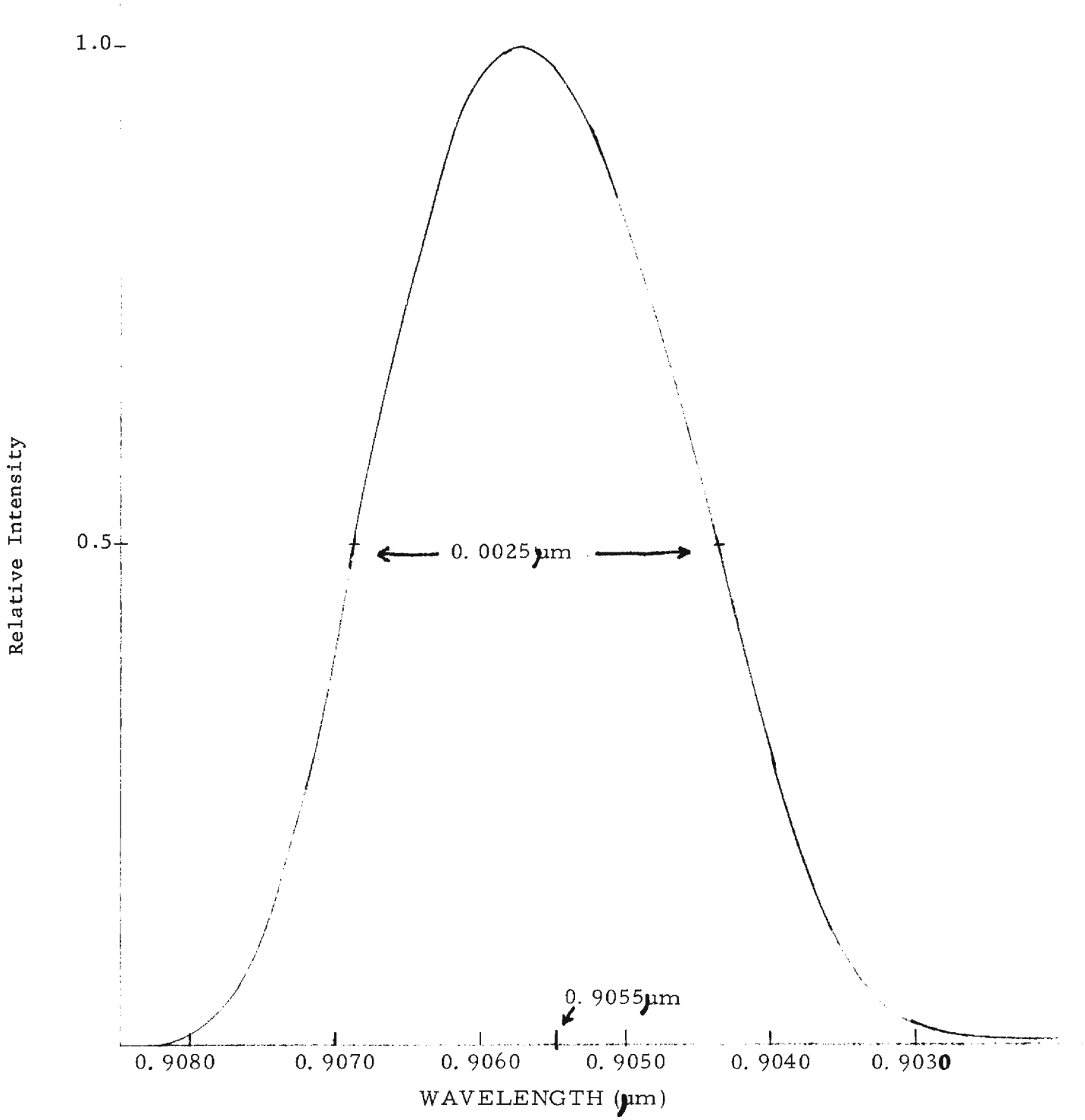

Figure 2.2. Power Spectrum of the LDL-65 GaAs Laser Diode

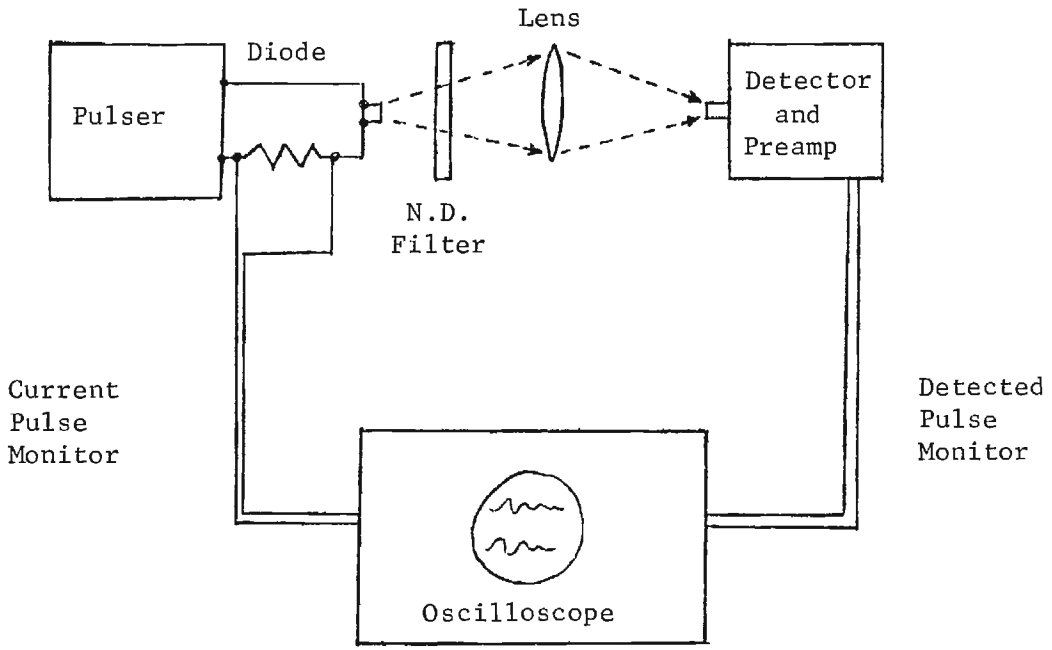

Figure 2.3. Measurement Set-Up for Measuring the Pulse Characteristics of the GaAs Laser Diode.

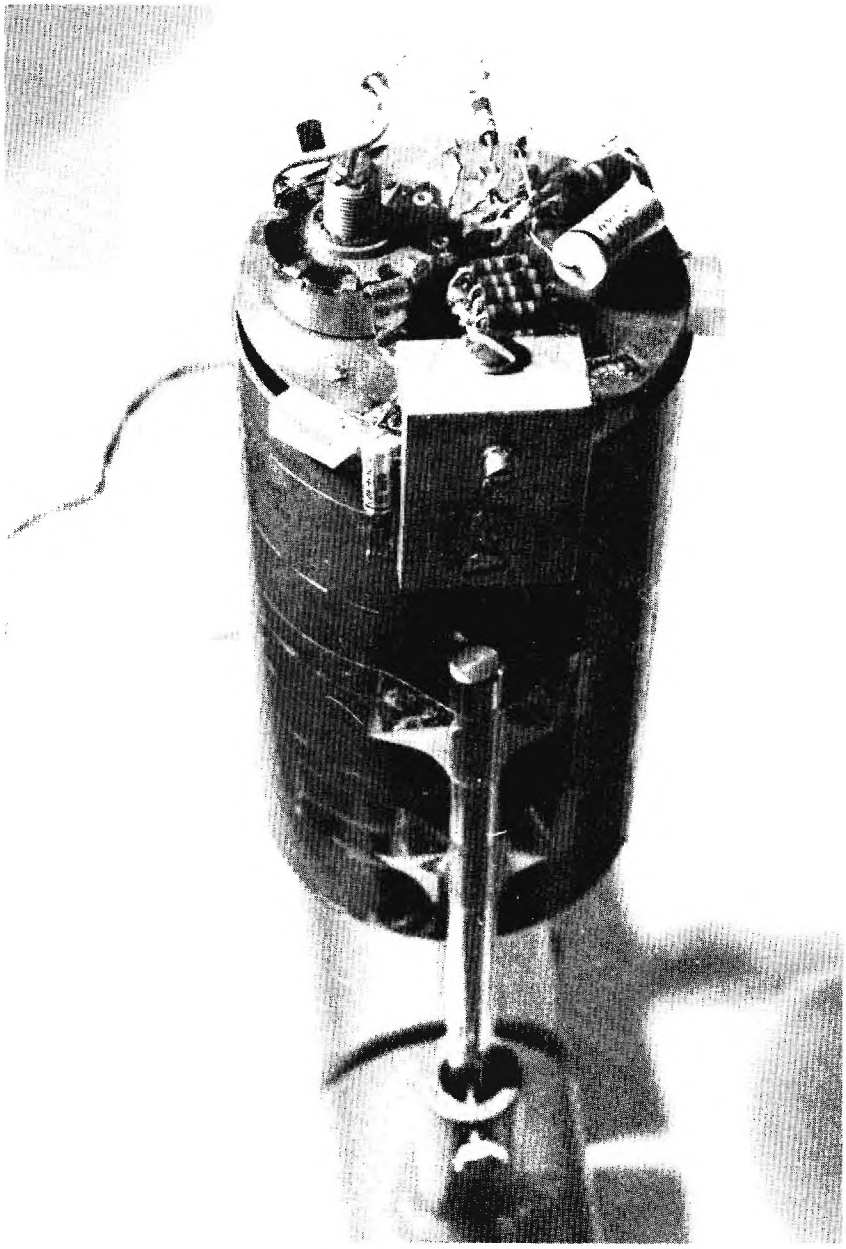

Figure 2.4. GaAs Laser Diode and Associated Driver.

The series resistance for measuring the pulse current was made up of several resistors in parallel in order to achieve a value less than 0.1 ohm. The paralleled resistors are located just behind the laser diode mounting bracket.

The oscilloscope display comparing the laser current pulse with the detected radiation pulse is pictured in Figure 2.5. The top curve represents the current through the diode laser as a function of time, for a single pulse. The vertical sensitivity was 10.7 Amperes/centimeter, and the horizontal time scale was 100 nsec/cm. The lower trace represents the signal from the PIN photodiode detector. The two important features of this photograph are the shapes of the pulses and the delay between the peak of the laser current and the peak of the detected signal. The 100 nsec delay is primarily due to the preamplifier and connecting cable because the distance between the laser and the detector was insignificant. A separation of 1 m would introduce a delay of only 0.1 nsec, and the actual separation was less than 1 meter.

The current pulse was about 200 nsec wide at the 3 dB points and the detected signal was only about 50 nsec wide. This was a result of the current pulse not being above the laser threshold value for the full 200 nsec.

2.3 Linearity of UDT 40A Radiometer

The United Detector Technology (UDT) Model 40A Radiometer was chosen as the standard instrument for measurement of 0.9 μm wavelength signal intensity in the laboratory testing and field testing phases of this program. The UDT 40A Radiometer combines a silicon PIN photodetector with a subtractive filter to achieve an essentially flat response from about 0.45 μm to 0.95 μm wavelength. The instrument is precalibrated and reads directly in microwatts over a dynamic range of 10^{-1} to 10^{4} microwatts when used with the 1 cm^2 photodiode. Absolute calibration of the radiometer was assumed from the published technical specifications applicable to this instrument and linearity of response was measured over the signal intensity range pertinent to this program.

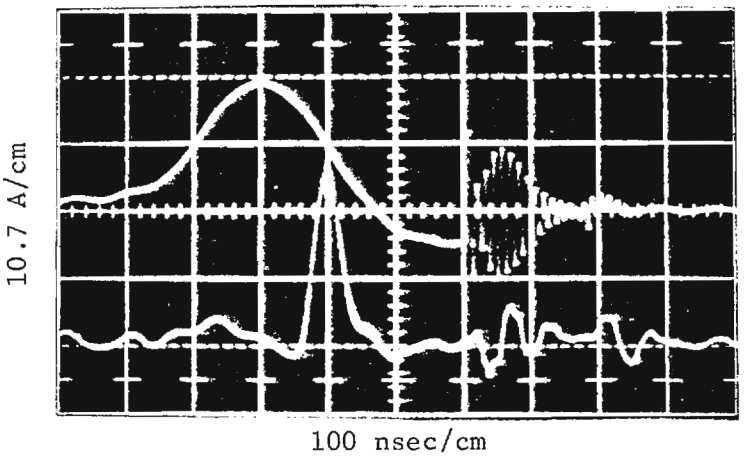

Figure 2.5. Pulse Response Characteristics of the GaAs Laser Diode.

In testing the fiber optic receptors, it was found to be convenient to perform some of the preliminary tests with visible radiation at 0.633 μm from a helium-neon laser. The linearity of the radiometer was, therefore, measured at both 0.633 μm and 0.9 μm. The method of measuring the linearity was the same in both cases. Calibrated attenuators in the form of neutral density filters were used to vary the power incident on the detector. The laser beams were diverged by lenses in order to cover the entire active area of the detector, as shown in Figure 2.6. A semi-log plot of the meter reading as a function of signal attenuation in dB was used to show the range of linear response of the radiometer.

The radiometer was tested over a 4 decade range of incident power. The range was limited by the attenuators available rather than by the sensitivity or nonlinearity of the radiometer. The results of these measurements which are shown in Figure 2.7 indicate that over the available range the response was essentially linear, even when changing from one meter range to another.

An experimentally convenient method for checking the linearity of response is to read the meter, insert a 3 dB attenuator, and observe the meter reading which should decrease by a factor of 2. This technique was used regularly when working with the diode laser source because the range of linear response varied as a function of the pulse parameters. This was expected because the detector element saturates at a certain peak intensity, whereas the meter indicates average intensity. As the pulse rep rate and pulse width are decreased, the average power is likewise decreased and the radiometer will saturate at a lower meter reading.

The UDT Radiometer was employed as a standard for calibrating an Optics Technology, Inc. (OTI) Power Meter both at 0.633 and 0.905 μm wavelength. The calibrated OTI Power Meter provided a means for carrying out simultaneous measurements in the laboratory and the field where the intensity detectors were required. The calibration with the helium-neon laser radiation at 0.633 μm was carried out over a 3 decade range. However, because of the limited sensitivity of the OTI Power Meter and the relatively low average power of the diode laser, the calibration at 0.905 μm could be

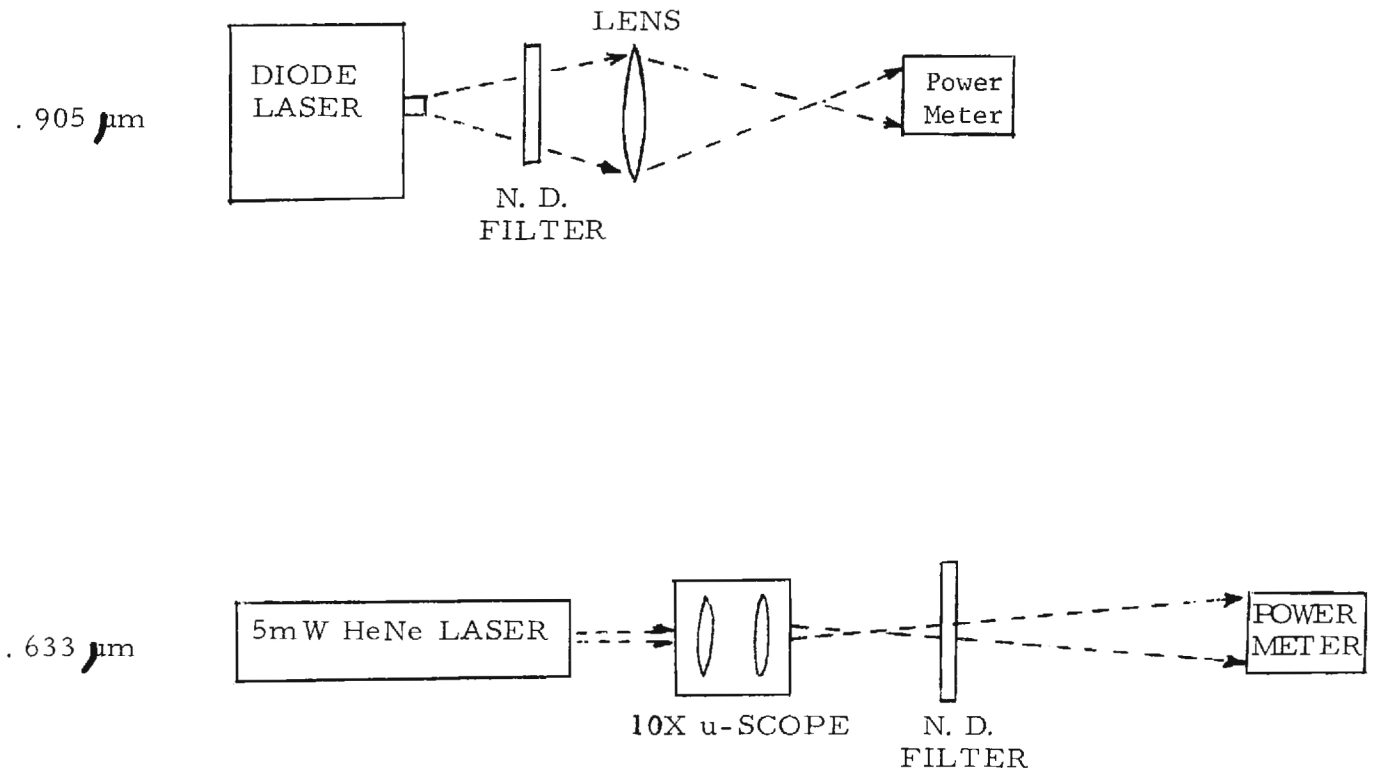

Figure 2.6. Experimental Setup Used to Determine the Linearity of the UDT 40A Radiometer.

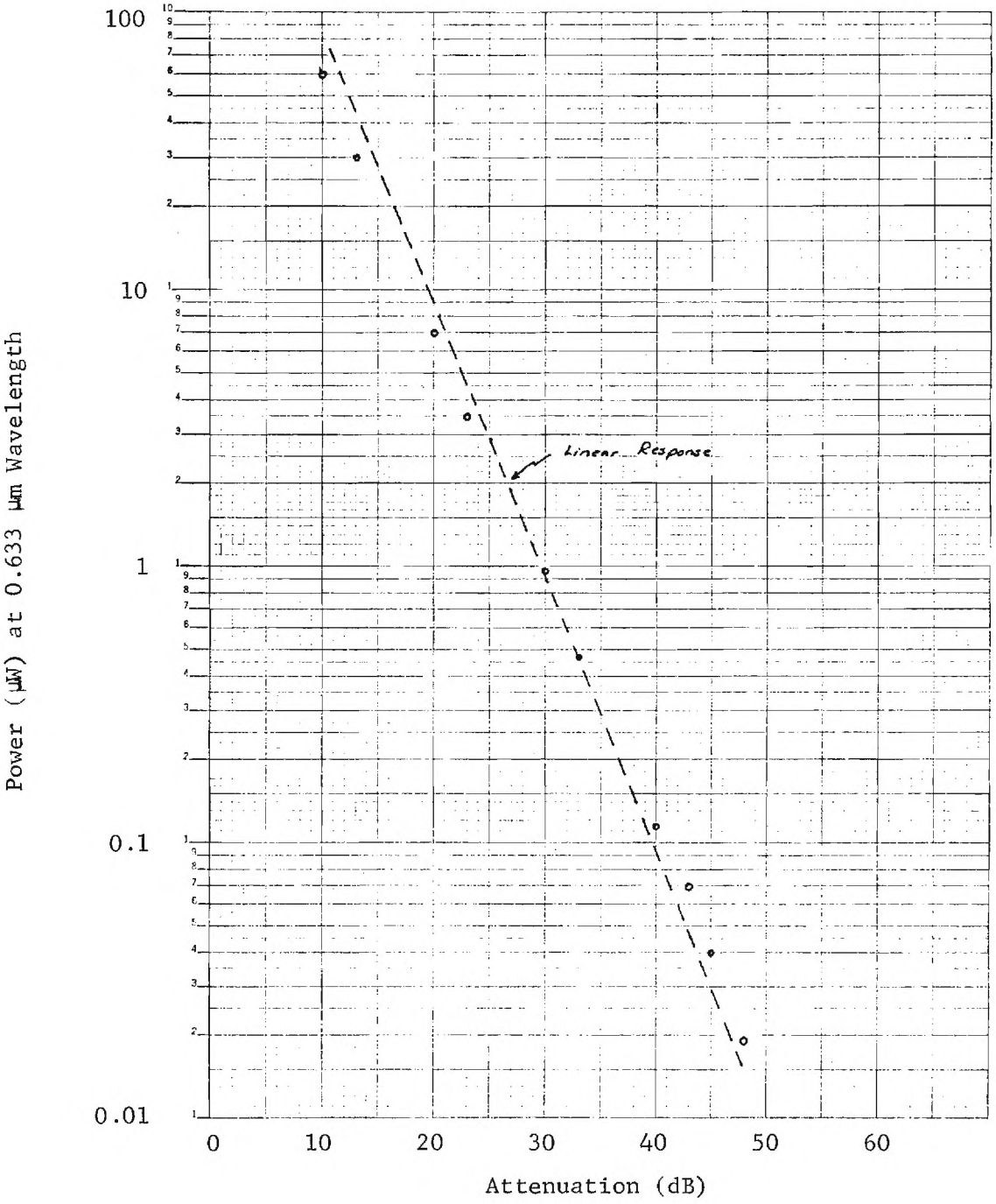

Figure 2.7. Linearity of the UDT 40A Radiometer.

accomplished over a range of only 1 decade. The linearity of response and the absolute calibration for the OTI Power Meter are shown in Figure 2.8 in which the meter reading for the OTI instrument is plotted against the reading of the UDT 40A Radiometer for the same input power levels.

2.4 Spectral Characteristics of Neutral Density Filters

The calibration of the neutral density filters which were utilized as attenuators in the linearity tests on the UDT-40A Radiometer was determined at 0.9 μm wavelength. The manufacturer's specifications for the spectral characteristics of the filters did not extend out to 0.9 μm so the % transmission was measured at this wavelength with a Perkin Elmer Spectrophotometer. The results indicated that the nominal values of optical density over the specified range in the visible spectrum were applicable at 0.9 μm wavelength. The results are shown in the table below:

Nominal O. D.	Measured T % at 0.9 μm	Measured O. D. at 0.9 μm
0.3	50	0.30
0.5	32	0.49
1.0	10	1.00

Optical density (O.D.) is defined as the logarithm of the reciprocal of the Transmission, T.

$$O.D. = \log \frac{1}{T}$$

Since attenuation in dB is defined as 10 times the log of $\frac{1}{T}$, attenuation in dB is 10 x O.D.

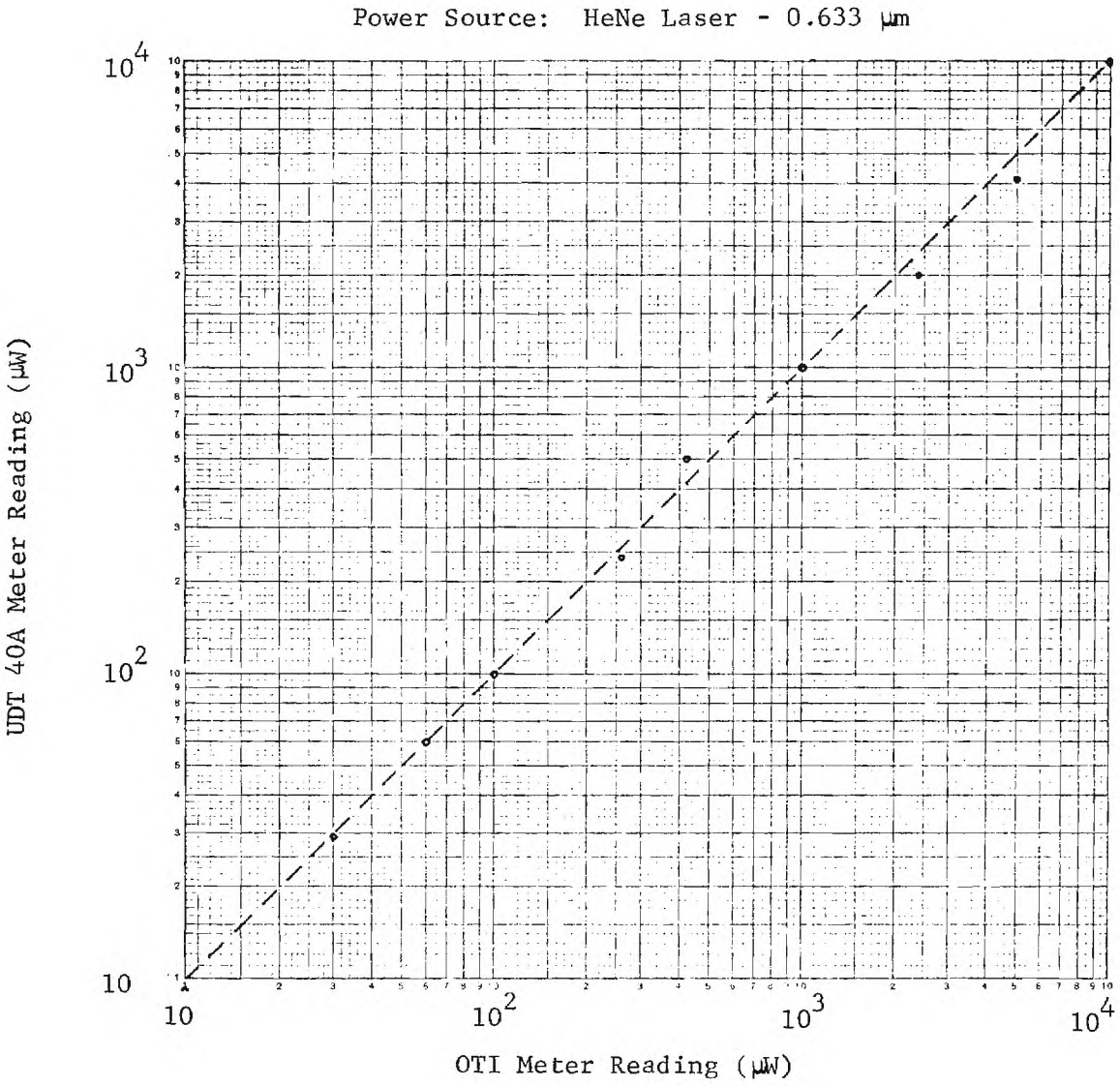

Figure 2.8. Absolute Calibration and Linearity of the OTI Power Meter.

3. OPTICAL PROPERTIES OF DETECTOR PANEL COMPONENTS

3.1 Optical Properties of Plastic Optical Fibers

3.1.1 Fiber Loss per Unit Length

In order to compare the relative merits of optical fibers of different types, a standard procedure was established for measuring the loss per unit length in units of dB/ft. The procedure consisted of coupling a source to one end of a fiber and measuring the power out of the other end of the fiber for different lengths obtained by cutting off successive increments of the original fiber. A graph of the data on semi-log paper was then fitted with a straight line whose slope yielded the loss per unit length.

Details of the experimental setup for measuring the loss/length of the optical fibers is shown in Figure 3.1. In this figure, a GaAs laser diode source is coupled into the fiber end with an f:1 lens whose angle of convergence approximately matches the mode of the fiber optic rod with the source and fiber located at a distance 2f from the lens plane. The input end of the fiber is held in a micrometer driven x-y-z stage to facilitate optimum coupling, and the output end is terminated into a PIN photodiode and fast response preamplifier.

A picture of the apparatus in a light-tight enclosure is shown in Figure 3.2. The source is the diode laser mounted on the delay line pulser at the left end of the figure. A neutral-density filter is located between the laser end and a converging lens. The input end of the fiber was fastened to the inverted-L-shaped rod which was mounted on the x-y-z micrometer stage.

The output end of the fiber was passed through a hole of comparable diameter drilled in a metal plate to block stray radiation. The radiometer detector was mounted behind this plate and was illuminated by the radiation transmitted by the fiber.

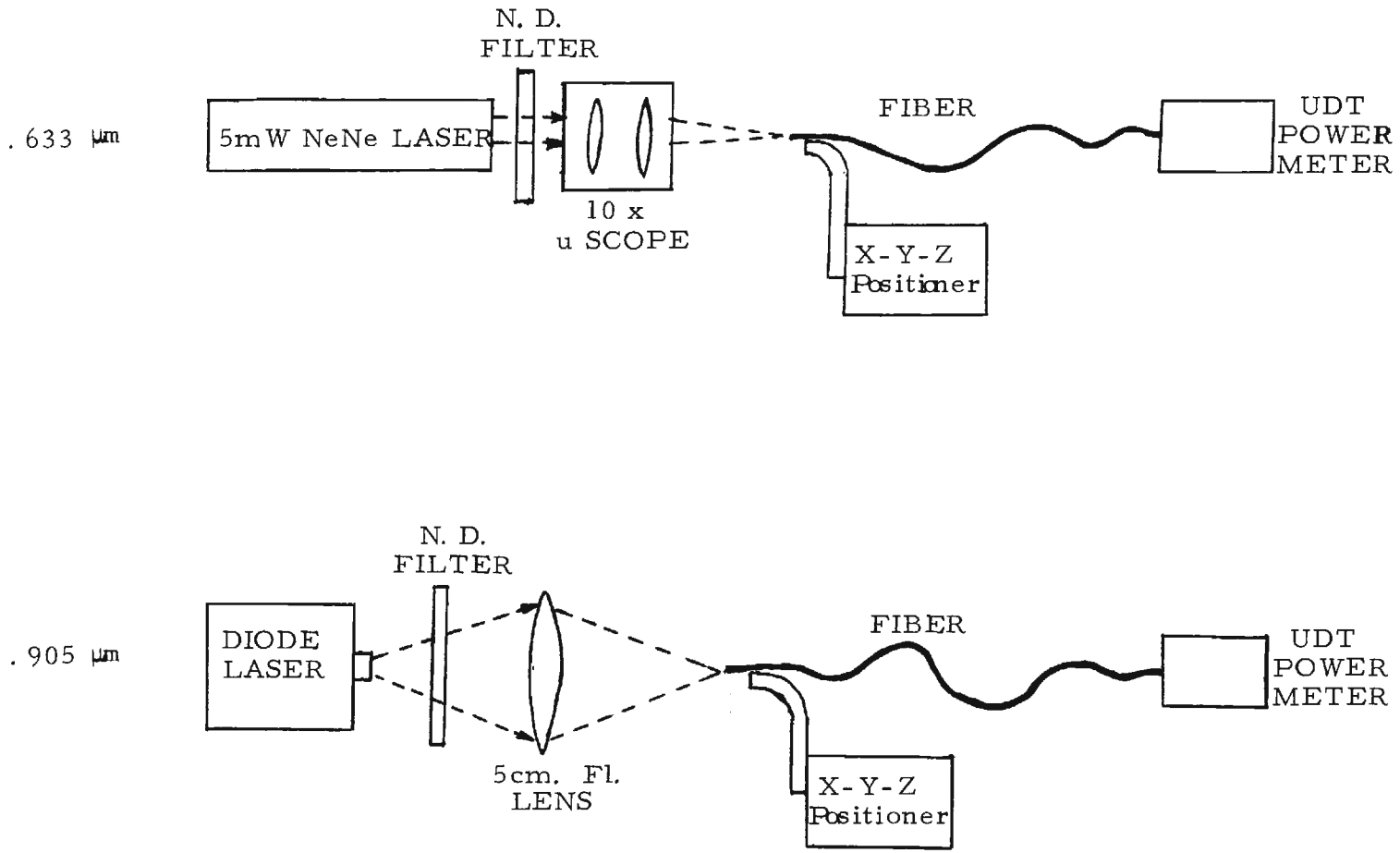

Figure 3.1. Experimental Setup for Measuring the Loss/Length in Optical Fibers.

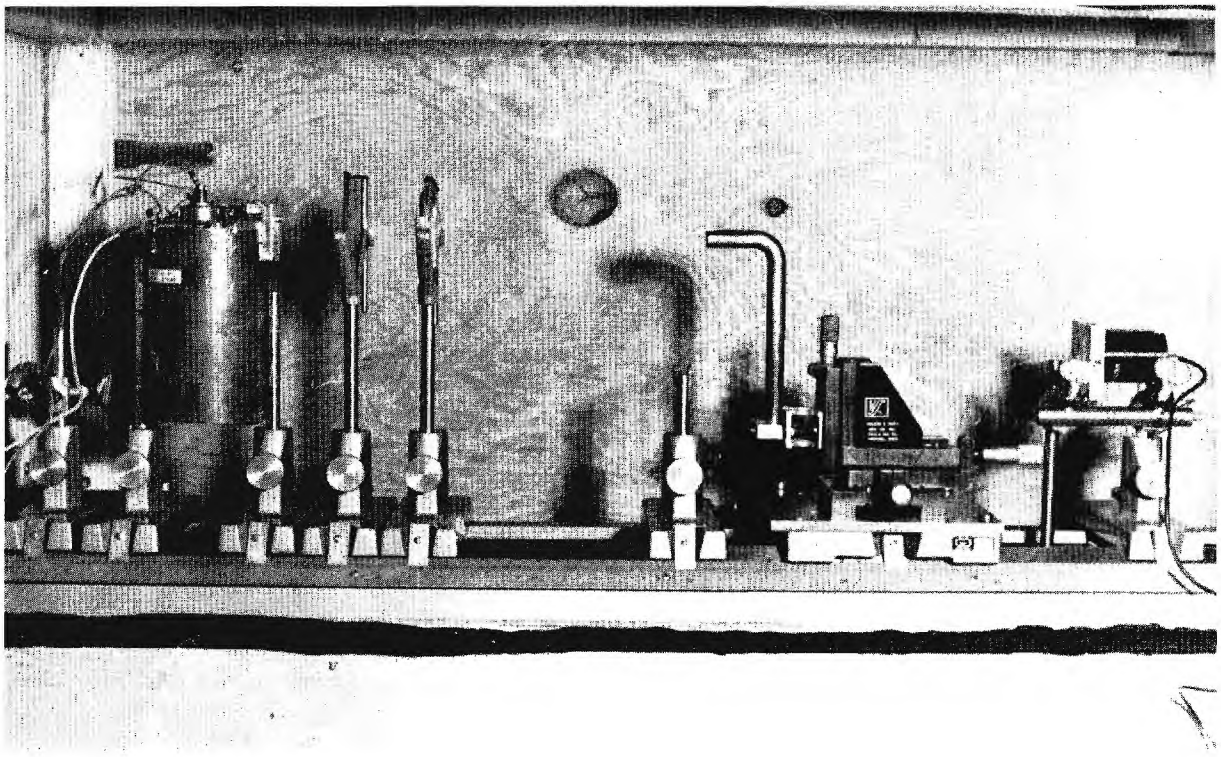

Figure 3.2. Photograph of the Optical Test Bench in a Light-Tight Enclosure.

The graphical data presentations were helpful for two reasons. First, the graphs revealed any unusual scatter in the data resulting from variations in the input or output coupling configuration or nonlinear detector response. Measurements indicating suspicious features were then repeated under improved conditions to assure linearity and minimum scatter of the data points. Second, the best fitting straight line through the data was used to obtain the values of loss per unit length and also of the incident power coupled into the fiber.

The measured values of loss per unit length for 0.633 μm and 0.9 μm radiation are tabulated in Table 3.1. In the initial tests it was found to be convenient to employ 0.633 μm visible radiation to provide a visual confirmation of the optimum position for the fiber relative to the coupling lens. As the tests progressed, however, a high level of confidence was acquired in locating the desired position by instrument readings obtained by moving the end of the fiber through a systematic search pattern about the focal point of the lens.

As expected, the data of Table 3.1 shows that the loss/length at 0.633 μm is less than that at 0.9 μm. It was, however, expected from Dupont's published technical literature on IRX (infrared transmitting) fibers that the loss/length at 0.9 μm for this fiber would be less than 3 dB/ft, whereas the actual measured loss was 8.5 dB/ft. On the other hand, it was not expected that the Poly Optics fiber would be competitive with DuPont's IRX since no claims were made by Poly Optics for performance outside the visible spectrum. In comparison, however, the measured loss for the 10 mil Poly Optics fiber at 0.9 μm was found to be 2.2 dB/ft. Technical discussions with both Poly Optics and DuPont, and spectrometric measurements performed during this program, have provided an explanation for the loss data. Figure 3.3 shows a transmission spectrum with resolution of about 0.01 μm for 10 mil diameter IRX and 10 mil diameter Poly Optics fibers. Note that adjacent maxima and minima are separated by about 0.02 μm, and that at the GaAs diode laser wavelength (0.905 μm) the IRX is near transmission minimum while the Poly Optics is near transmission maximum. Figure 3.4 shows an extended spectrum for the Poly Optics fiber from which the sharp onset of

TABLE 3.1

FIBER LOSS PER UNIT LENGTH

Wavelength	Fiber		Loss/Length (dB/ft.)
	Type	Diameter (mils)	
0.633 μm	DuPont Regular Crofon	20	1.1
0.633 μm	DuPont Regular Crofon	10	0.3
0.633 μm	DuPont Crofon IRX	10	1.5
0.633 μm	Poly Optics	10	0.8
0.633 μm	Poly Optics	20	0.3
0.905 μm	DuPont Crofon IRX	10	8.5
0.905 μm	Poly Optics	10	2.2
0.905 μm	Poly Optics	20	1.9

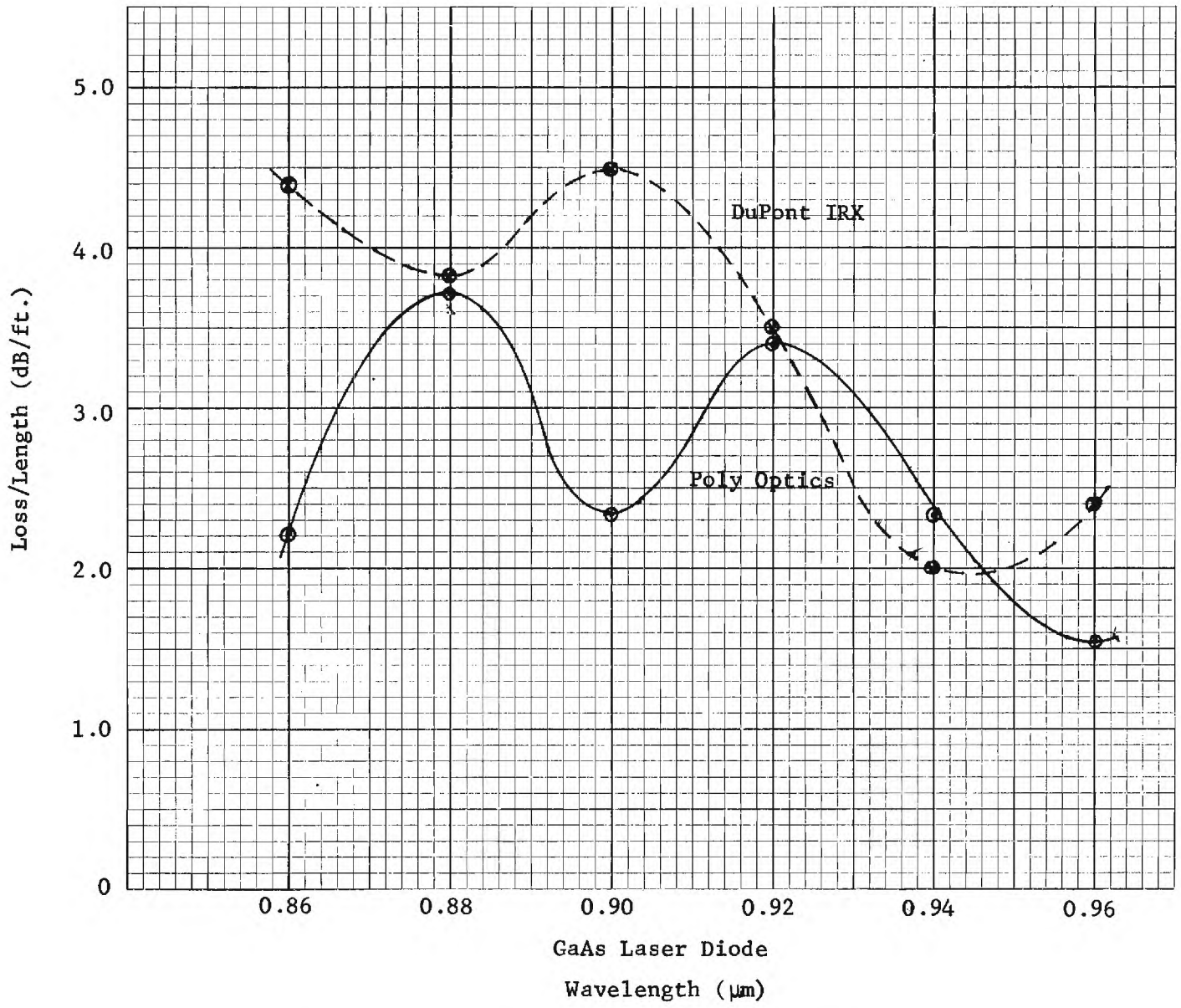

Figure 3.3. Transmission Spectrum of Two Plastic Optical Fibers.

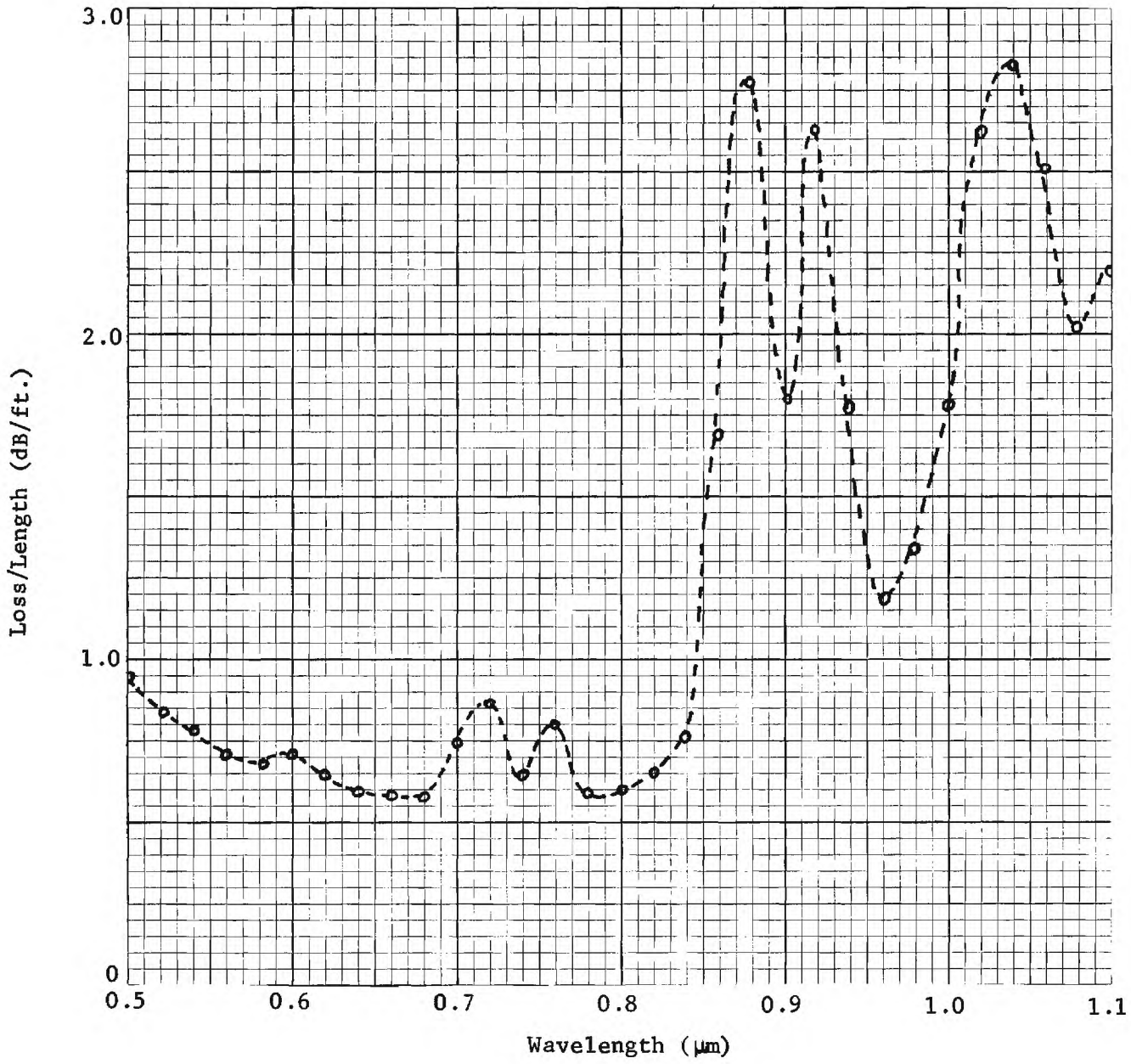

Figure 3.4. Transmission Spectrum of 10 mil Diameter Poly Optics Optical Fiber.

absorption is shown to occur at about 0.84 μm as the wavelength increases from the visible spectrum into the infrared. Apparently the location of the maxima and minima depend on the composition of the plastic core material, and the Poly Optic formulation results in good transmission at the narrow line diode laser wavelength. DuPont says that their IRX fiber is intended for use with light emitting diodes (LEDs) whose peak wavelength falls at about 0.94 μm and whose linewidth is about 0.06 μm. From the spectrum of Figure 3.3, it can be seen that the IRX fiber has a transmission maximum at this wavelength. Data published by DuPont on the IRX fiber was taken with a spectrometer whose resolution was about 0.05 μm, and thus much of the structure shown in Figure 3.4 was averaged out. For applications requiring the use of plastic fibers with narrowband laser diode radiation, high resolution spectra are needed.

In order to measure the effect of extreme temperatures on the transmission loss of the optical fibers, the middle 4 foot section of a 6 foot long fiber was coiled up and immersed in fluids at different temperatures.

There was no measurable change in the power transmitted at 0.9 μm by the fiber when the air around the coiled section was replaced with water at 27°C (81°F). Likewise, there was no change when this water was replaced with ice water at 1°C (34°F). When the ice water was replaced with water at 75°C (165°F), there was only a slight increase (less than 0.03 dB) in the power transmitted. The fibers distort at temperatures around 88°C (190°F).

The output power did not change significantly until the fiber was immersed in the cold gas from liquid nitrogen. When the fiber was immersed in the liquid nitrogen itself, the power transmission was decreased by only 2.7 dB. It is not likely that a man wearing a fiber optic vest would ever be exposed to the extreme temperature of liquid nitrogen; however, even at that temperature, the additional loss is less than 3 dB.

3.1.2 Fiber Loss vs. Bend Radius

Since the fiber optic panel was configured so that the optical fibers terminated perpendicular to the front surface of panel and ran parallel with the back surface, a 90° bend in the fiber was required. The losses

introduced by bending an optical fiber were measured by a comparison technique. First, using coupling techniques previously described for the loss/length measurements, the output power from a straight fiber was measured for use as a reference. Then, the output power was measured for each of four 360^{o} bends formed around a metal rod, as indicated in Figure 3.5. The rod was machined to have four sections of diameter: 0.1, 0.2, 0.3 and 0.5 inches. The first bend around the rod was made on the 0.5 inch diameter segment and each succeeding bend was made around a smaller diameter segment. The bend loss in dB was then calculated by

$$\text{Bend Loss (dB)} = 10 \log \frac{P_{straight}}{P_{bent}}$$

where $P_{straight}$ was the power output of the straight fiber and P_{bent} was the power output of the bent fiber. The results of these measurements and calculations are shown in Table 3.2 for radiation of 0.633μm wavelength from a helium-neon laser. Each value represents the average of five samples.

It is seen that the loss introduced by a bend increases as the bend diameter decreases. Also, at this wavelength, the DuPont IRX fiber displayed the lowest bend losses, while the Poly Optics 20 mil diameter fiber showed the greatest bend losses. Comparing the data for the two different sized Poly Optics fibers reveals that the larger the fiber diameter, the greater the loss in a bend of a given diameter. A general rule is that losses due to bending are not significant for bends of radius greater than 10 times the fiber diameter. The data of Table 3.2 shows that the bend loss is less than 1dB for all cases where the above rule is satisfied.

The bend losses at 0.905μm wavelength, which are tabulated in Table 3.3, are significantly different from those at 0.633μm. The DuPont regular Crofon fiber was not expected to perform well at this wavelength and its high values of bend loss are not surprising. Also, in view of the comparitively higher scattering and absorption losses, it was disappointing, but not surprising, that the bend losses for the DuPont IRX fibers are higher than those for the Poly Optics fibers. For both the 10 mil and 20 mil diameter Poly Optics fibers, the loss for a bend whose diameter is equal to 10 times the fiber diameter is about 1dB.

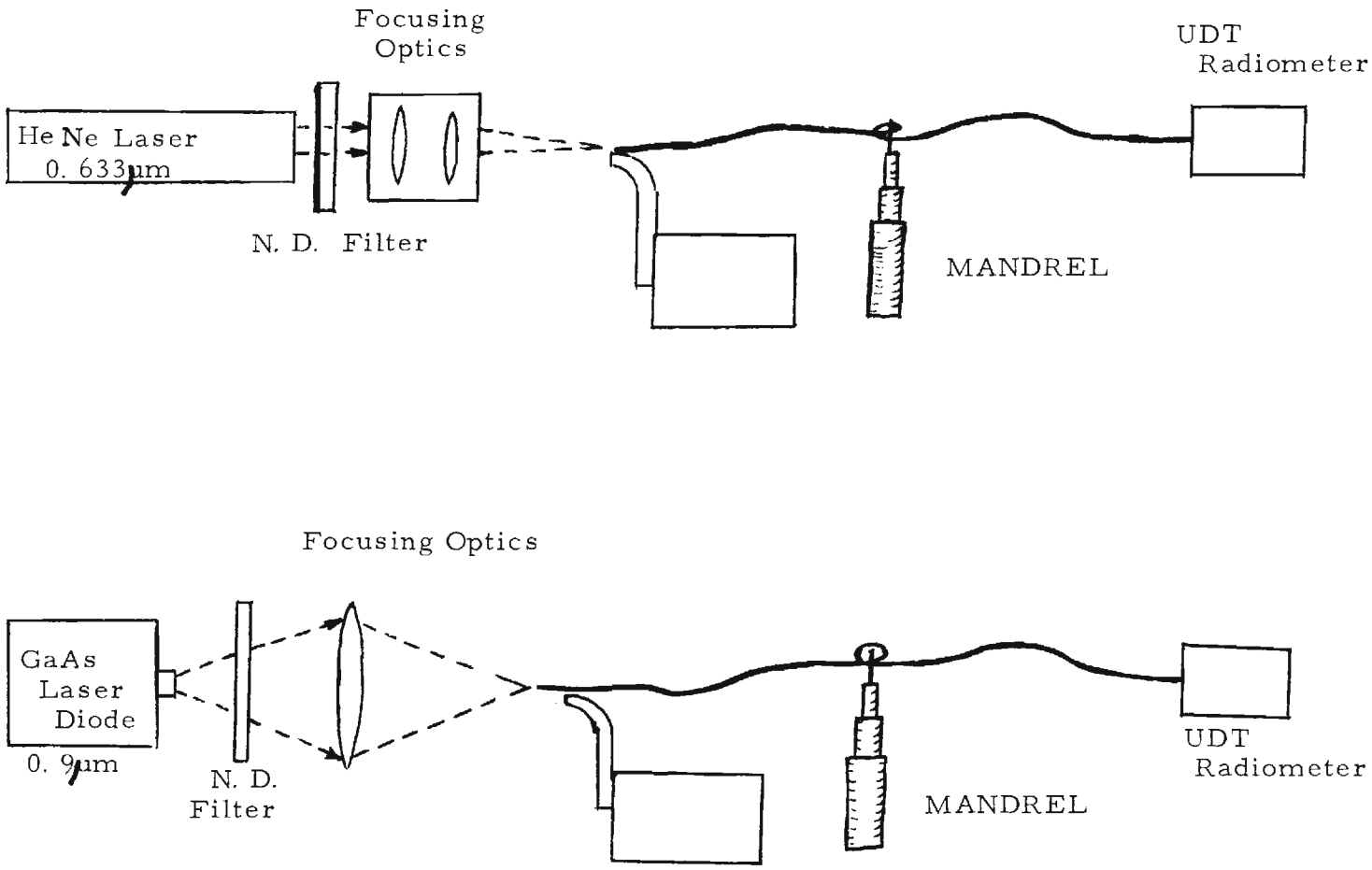

Figure 3.5. Sketch of the Experimental Setup for Measuring the Bend Loss of Optical Fibers.

TABLE 3.2

Bend Losses at 0.633μm Wavelength

Fiber / Bend Diam. (in.)	0.5	0.3	0.2	0.1
DuPont Regular Crofon 10 mil diam.	0.09dB	0.14dB	0.22dB	0.67dB
DuPont Crofon IRX 10 mil	0.02	0.05	0.12	0.43
Poly Optics 10 mil	0.04	0.06	0.15	0.80
Poly Optics 20 mil	0.14	0.37	0.85	1.72

TABLE 3.3

Bend Losses at 0.905μm Wavelength

Fiber \ Bend Diam. (in.)	0.5	0.3	0.2	0.1
DuPont Regular Crofon 20 mil diam.	6.8dB	16.0dB	19.0dB	23.8dB
DuPont Crofon IRX 10 mil	0.5	1.4	2.9	4.3
Poly Optics 10 mil	0.1	0.1	0.2	1.0
Poly Optics 20 mil	0.1	0.2	1.0	2.2
Poly Optics - 20 mil Potted with Epoxy	3.1	5.2	8.2	11.3

Measurements were also made to determine the effects of potting the fiber bends with epoxy. These measurements were made in the same manner as those discussed above with the bends potted to the bend forming rod. The results are presented in Table 3.3 for 20 mil Poly Optics fibers at 0.9μm wavelength. The additional loss caused by potting the bend is much greater than that caused by potting the straight sections because the fields extend further outside the cladding in the bend and hence the coupling is much easier to perturb by wetting the fiber. It was found, however, that the additional loss incurred in the 360^{o} was much greater than that incurred in the 90^{o} bend configuration employed in fabrication of the end-coupled array panels. Tests performed on potted 90^{o} bends showed that a loss of 6dB is obtained on 20 mil Poly Optics fibers bent to a diameter of 0.1 inch. The conclusions drawn from these measurements is that wetting the optical fibers with potting compounds whose index of refraction are of the order 1.5 or greater will result in unacceptable losses in both the bends and straight sections. If epoxy is to be used in the fabrication of the target panel, it should be applied sparingly only along the straight sections of the optical fibers.

After measurements indicated that the bend losses were significantly larger for potted bends, the loss/length of a potted, but unbent, section of fiber was measured. The loss/length was measured to be 3.6dB/ft for the potted 20 mil Poly Optics fiber. The loss/length for 20 mil Poly Optics fibers in air was measured to be only 1.7 dB/ft. So, even though the fibers consist of a core material covered with a cladding of lower refractive index, the guided energy can still be absorbed and/or scattered at the outer surfact of the cladding material. Apparently the fields extend for at least several wavelengths outside the cladding, and any fluid which wets the cladding and which has a dielectric constant close to that of the cladding causes the radiation loss at the interface to be increased.

3.1.3 Angle of Acceptance

Preliminary to the measurements at 0.9μm wavelength the radiation acceptance patterns for two Poly Optics fibers were measured at 0.633 μm wavelength. The beam from a helium-neon laser was directed toward one end

of a single optical fiber which was mounted on an optical bench coincident with the laser beam axis. The end of the fiber intercepting the radiation was mounted on a graduated rotating mount and the other end of the fiber was used to direct the radiation coupled into the fiber to the radiometer detector. The power output of the fiber was measured as a function of angle of incidence of the laser beam and the results used to determine the angle between the half power points of the radiation pattern.

The radiation patterns of a 10 mil diameter and a 20 mil diameter fiber are shown in Figure 3.6. The 0^{o} position of the rotator was not set accurately to correspond to the laser beam axis resulting in a slight angular offset of the pattern. The important information in this representation is the shape of the pattern and the angle between points where the power is 3dB down from the peak value.

Figure 3.7 shows the radiation pattern at 0.633μm of a 20 mil diameter fiber terminated on a woven mat. The termination was formed by epoxying one end of the fiber to the mat with the fiber axis perpendicular to the mat. The fiber behind the mat was then bent to lie parallel to the plane of the mat and was potted to the mat. This was one of several basic configurations which were investigated for terminating the optical fibers in a suitable fabric, and these configurations are discussed in greater detail in Section 4.1.

The mat and fiber were mounted to the graduated rotator with the axis of rotation parallel to the axis of the fiber which was potted to the back surface of the mat. The angle of acceptance for rotation about this axis is shown in the upper part of Figure 3.7 and is essentially the same as that shown in Figure 3.6.

The bottom curve of Figure 3.7 is quite different, however, and illustrates one of the consequences of loss in the fiber bend. For this case the mat and fiber were mounted with the axis of rotation perpendicular to the previous axis but still in the plane of the mat. In this case the angular offset of the pattern is <u>not</u> due to an alignment error but due to radiation coupling through the fiber bend <u>over</u> the range of angles for which the bend was exposed to the laser beam.

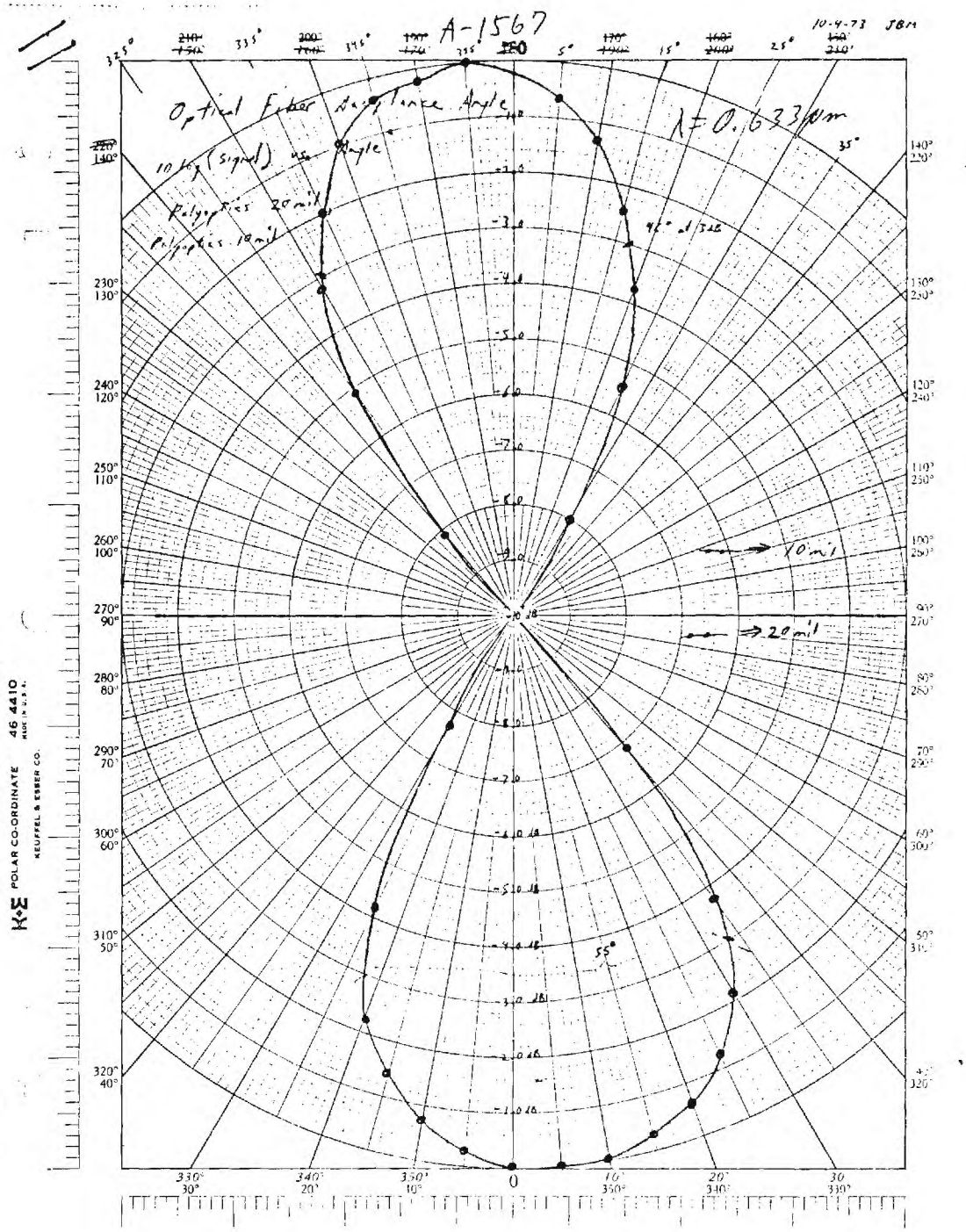

Figure 3.6. Angle of Acceptance of 10 and 20 mil Optical Fibers at 0.633 μm Wavelength.

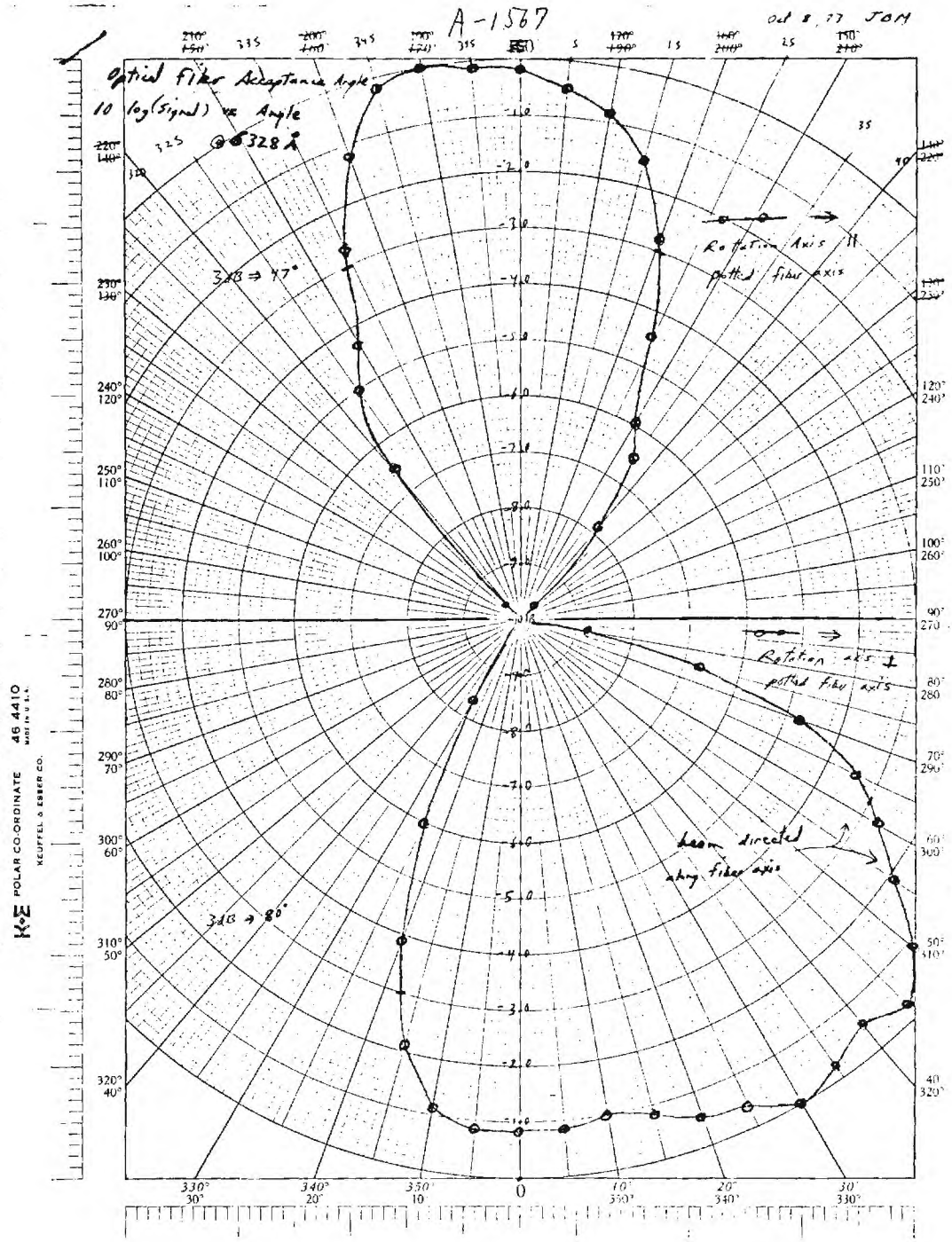

Figure 3.7. Angle of Acceptance of a 90° Bend Terminated Optical Fiber at 0.633 μm Wavelength.

Similar patterns were obtained at 0.9μm wavelength, as indicated in Figure 3.8. Here the zero degree line has been shifted in the graph by 30^{o}, but the results are essentially the same as in Figure 3.7.

The radiation acceptance pattern was also measured for a termination that consisted of a reflector at 45^{o} with respect to the incoming radiation, and a fiber whose axis was perpendicular to the radiation. The termination, which is illustrated in Figure 3.8, was designed to eliminate the optical fiber bend in the termination described above.

The radiation acceptance pattern was measured for two orthogonal axes of rotation, similar to those used for the potted, bent fiber termination above. The top curve of Figure 3.10 shows the pattern obtained by rotating the termination about an axis parallel to the fiber axis. The bottom curve shows the pattern for rotation about an axis perpendicular to the fiber axis. As expected, the two curves are essentially the same.

3.2 Optical Properties of Bonding Materials

The transmission of encapsulants and optically transparent tapes used to fabricate the candidate optical fiber sample inserts was measured to insure that their loss would not be prohibitive at 0.9μm wavelength. The results of these measurements are shown in Table 3.4.

All transparent encapsulants and tapes tested were shown to have acceptable low losses at 0.9μm wavelength.

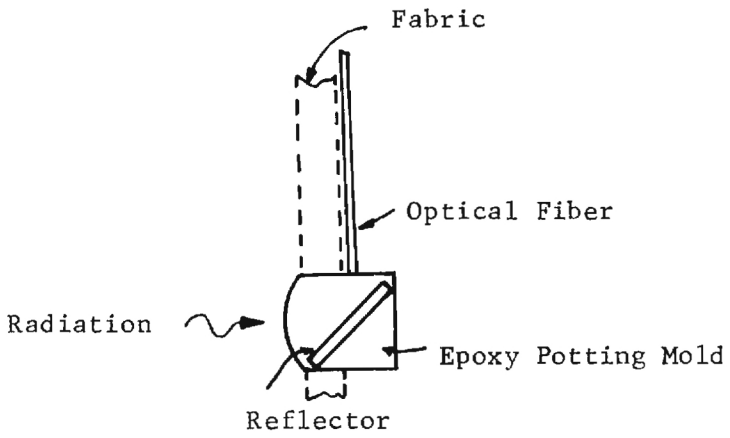

Figure 3.8. Drawing of the Reflector Terminated Optical Fiber.

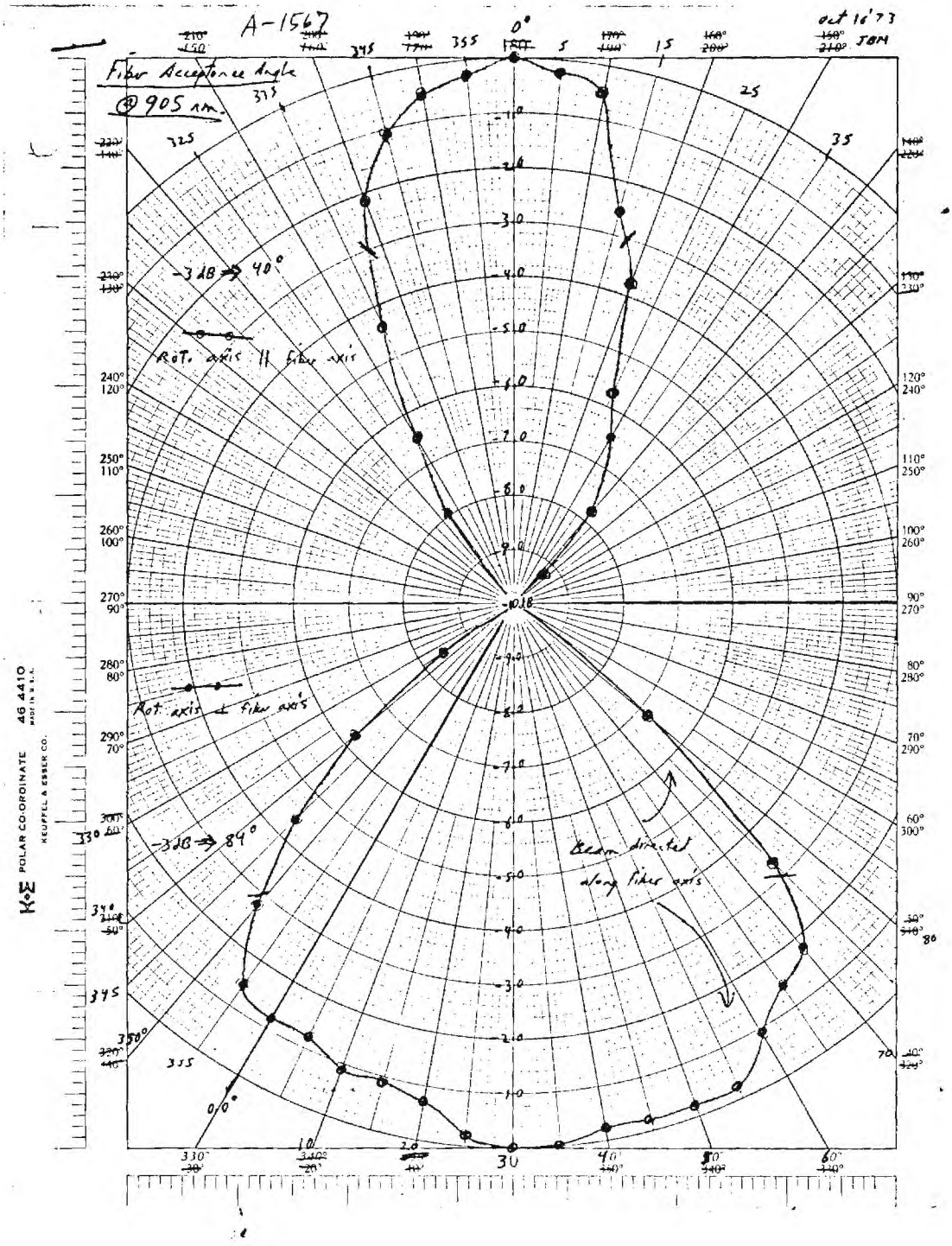

Figure 3.9. Angle of Acceptance of a 90° Bend Terminated Fiber at 0.9 μm Wavelength.

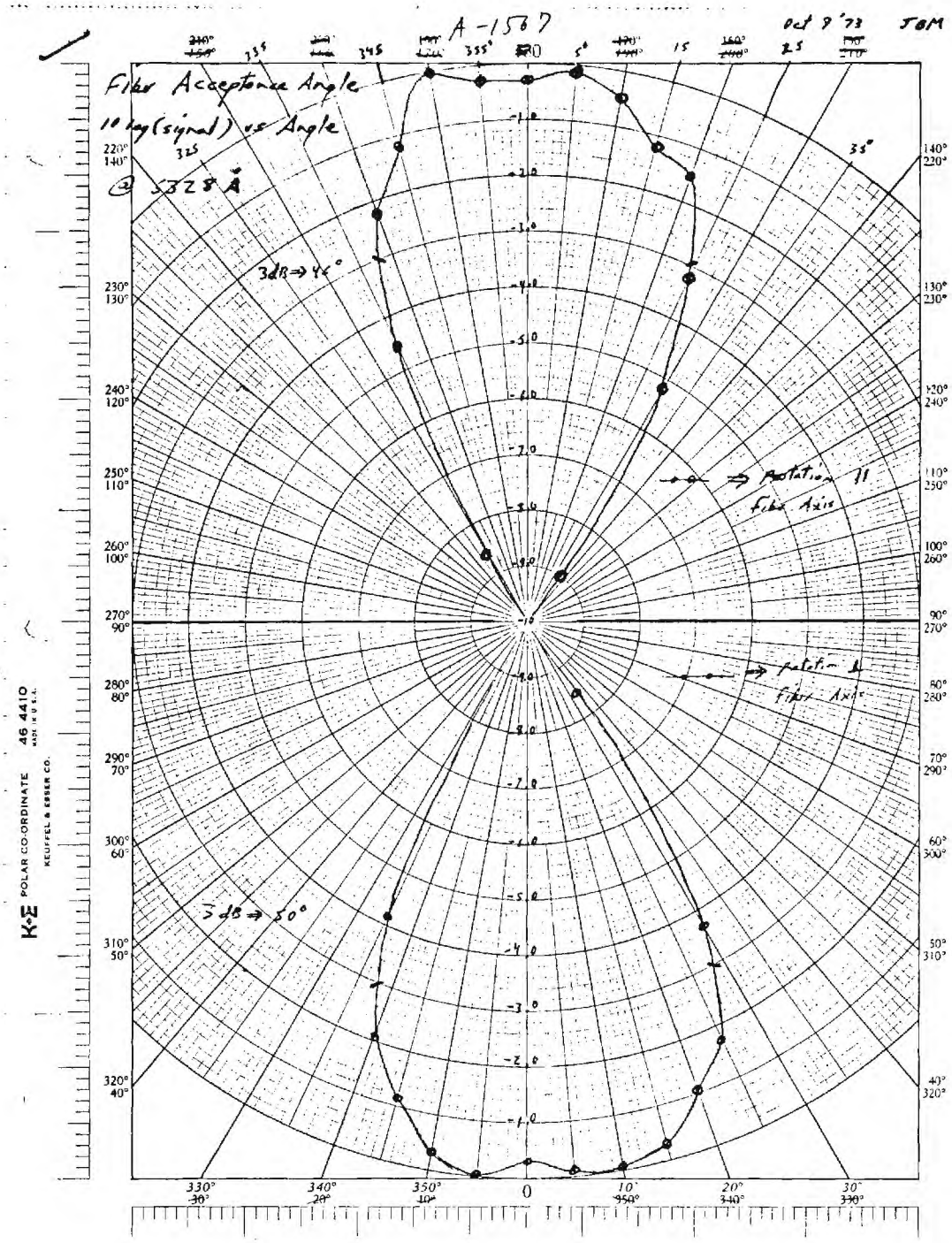

Figure 3.10. Angle of Acceptance of a 45° Reflector Terminated Optical Fiber at 0.633 μm Wavelength.

TABLE 3.4

Transmission Loss of Encapsulants and Tapes at 0.9 μm Wavelength

Material	Transmission Loss
TRA-CON Transparent Epoxy Type 2114	0.4dB/mm
Scotch Type T-8560 Tape	0.2dB/layer
Scotch Type 473 Tape	0.3dB/layer
Scotch Type 471 Tape	0.2dB/layer

4. DEVELOPMENT OF AN END-COUPLED FIBER OPTIC DETECTOR PANEL

4.1 Evaluation of Fiber Coupling and Implantation Techniques

A number of different fiber implantation techniques were evaluated by fabrication and testing of one or two samples of each technique. The purpose of these tests was to determine the most promising implantation technique consistent with the goals of: ease of fabrication, good optical performance, low detector panel thickness and good mechanical performance. The optical performance of these samples is discussed in Section 3.1.3. In general, the optical properties are the same for all samples which are end-coupled and terminated by a 90 degree bend into the panel. The performance of the reflector terminated sample was found to be very close to that of the unbent single optical fiber.

1. Single Fiber Machined Insert - A 3/16" diameter acrylic rod was cut into 3/16" long lengths which were drilled lengthwise .0225" d. A .020" d fiber was inserted through the insert and bonded with Duro-5 Minute Epoxy. Once the epoxy set, the fiber was cut with a sharp razor blade. Optical performance was good. Time required to fabricate inserts was longer than desired. A photograph of this sample is shown in Figure 4.1.

2. Multiple Fiber Machined Insert - This insert was identical to the single fiber insert except the hole was larger and four .010" d fibers were inserted and bonded into place. Performance was inferior to the single fiber insert and fabrication was more difficult.

3. 90^{o} Reflected Insert - In this technique a mirror was placed in a machined groove 45^{o} to the detector surface. A .020" d fiber was inserted through a drilled hole parallel to the detector surface. The mirror and fiber were bonded into place with Duro-5 Minute Epoxy. Performance was inferior to the single fiber insert, in that the angle of acceptance was limited by the size of the reflector. The thickness and complexity were considerably greater than the single fiber insert. Both front and back silvered mirrors

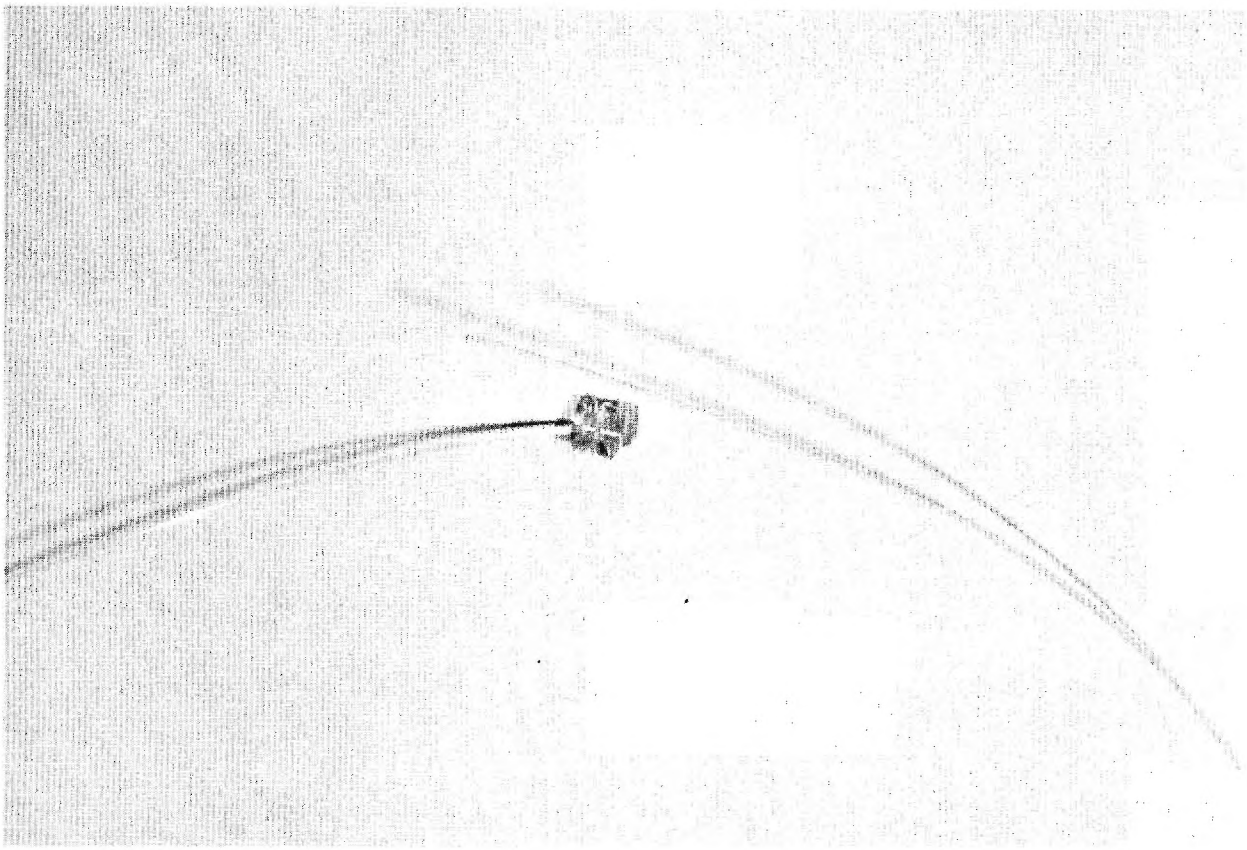

Figure 4.1. Single Optical Fiber Machined Insert.

were used with similar results. A photograph of this sample is shown in Figure 4.2.

4. Molded Epoxy Insert, Encapsulated Bend - This approach was an attempt to duplicate the insert used in #1 above without having to machine the insert. This technique was indeed much easier than anything tried previously. Since the bend radius tests indicated that losses due to bend radius were small, extensive optical tests were not performed on this sample. This technique was used to fabricate the initial panel. Only after results from the initial panel proved disappointing were extensive optical tests conducted. Tests showed that encapsulated bend losses were significantly higher than non-encapsulated losses. A photograph of this sample is shown in Figure 4.3.

5. Molded Matrix Detector Panel - This panel was fabricated by molding a 6 x 6 matrix of fiber optics on 1" centers into a 7" x 7" x 7/16" thick slab of GE RTV 615 flexible clear silastic. The idea behind this design was that panels could be clipped onto a vest much as armor or could be used in larger sizes or in groups as detector panel for vehicles. Optical tests of the panel indicated acceptable sensitivity. Apparently the RTV 615 and the modest bend radii used did not significantly increase the fiber losses. A photograph of this sample is shown in Figure 4.4.

6. Molded Epoxy Insert - Non-encapsulated Bend - This approach duplicated the implantation technique used in #4 except that the bend was not encapsulated and was made after the epoxy hardened. Optical tests indicated this method resulted in very low losses. This technique was used on the final test panel. Photographs of this fabrication technique are presented in Section 4.2.

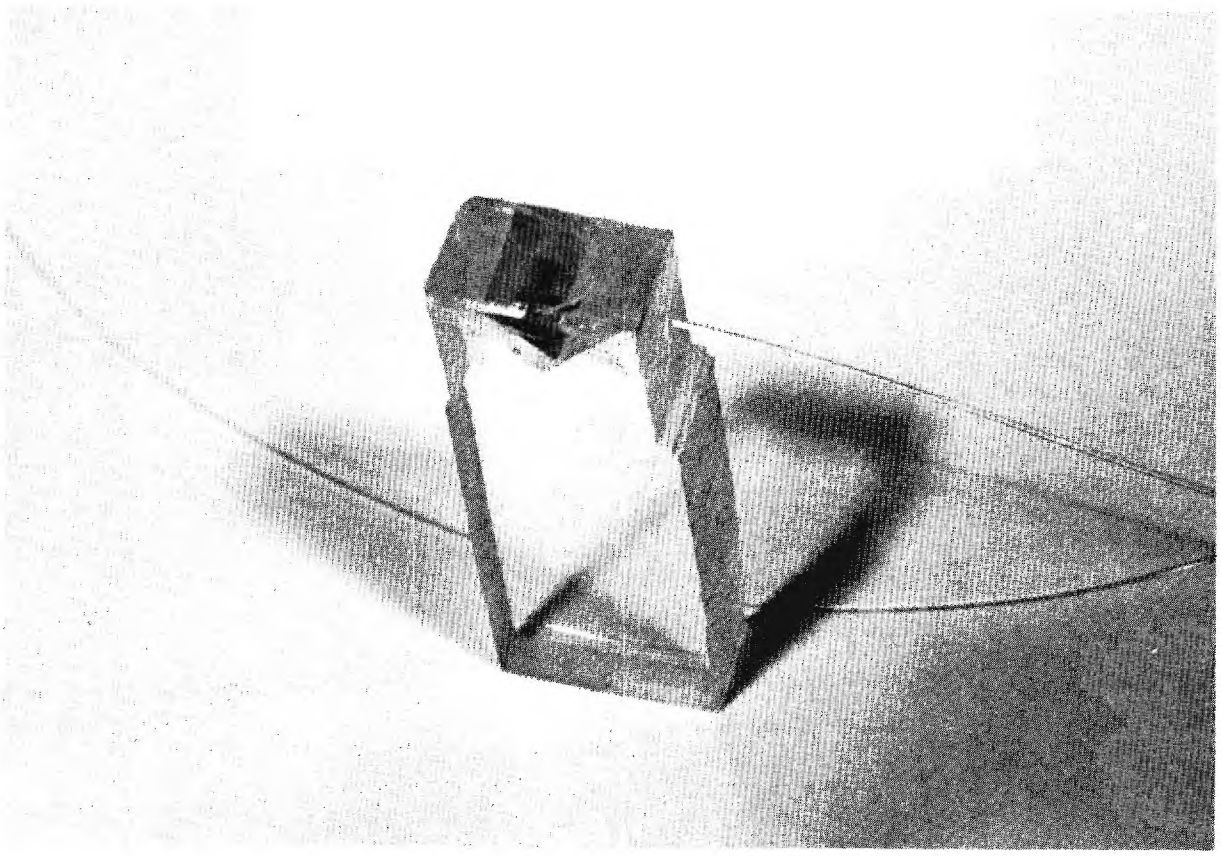

Figure 4.2. Reflector Terminated Optical Fiber Insert.

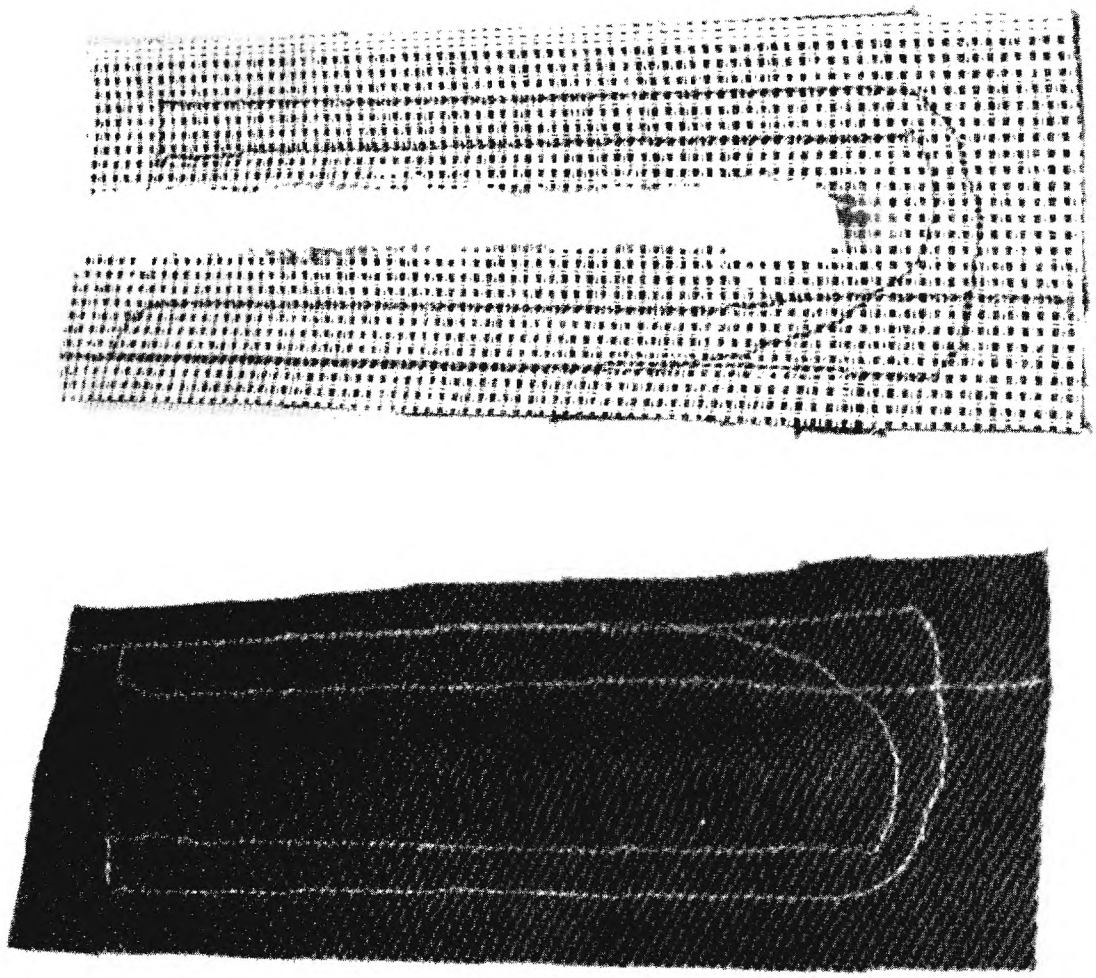

Figure 4.3. 90° Bend Terminated and Encapsulated Optical Fiber Insert.

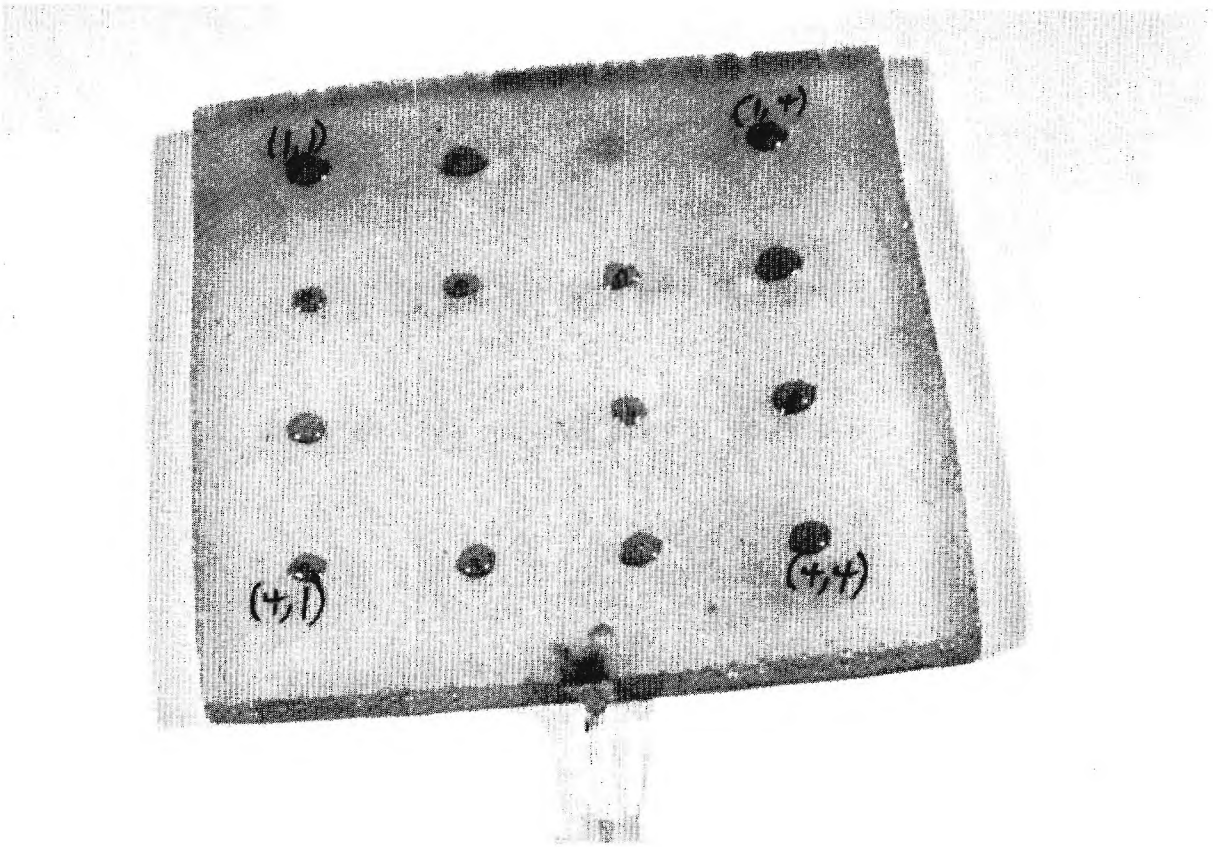

Figure 4.4. Molded Matrix Detector Panel.

4.2 Detector Panel Fabrication Techniques

4.2.1 Interim Fiber Optic Detector Panel

The first panel (Test Panel A) was fabricated by placing the vinyl covered cotton canvas over a teflon plate which had been predrilled with .0225 inch diameter holes spaced on 1 inch centers in a 12 x 16 matrix. The fibers were inserted through the teflon plate, through the canvas, and bent to run in rows parallel to the canvas surface. A fast-setting epoxy (Duro 5 Minute) was used to pot the bend where the fibers curved to parallel the canvas. Once all the fibers were located and fixed by the epoxy, each row was encapsulated with Dow Corning RTV 732 silicone potting compound. A machined Teflon mandril was used to form the silicone into hemicylinders over each row of fiber optics.

The canvas and fibers were then removed from the Teflon plate fixture and the fiber ends which had projected through the teflon plate were trimmed with a new razor blade. A medium-weight cotton denim was placed over the side of the panel containing the encapsulated rows of fibers and sewed into place using multifilament polyester thread. A row was sewed between each row of fibers and around the perimeter of the panel. All of the fibers ends were gathered and potted into an aluminum fitting. Figure 4.5 shows a close-up photograph of about one-half the panel front surface revealing the stitching pattern and the fiber optic end terminations. The complete panel with the fiber bundle termination connected to the illuminator used to test the panel's optical performance is shown in Figure 4.6.

Several problems were noted with this panel. The silicone potting compound bled through the canvas, causing the panel to have a poor appearance from the front side. Additionally, it was observed that when the fibers were illuminated from the fitting end in a dark room, considerable losses were observed, not only at the bends, but, to a lesser extent, all along the encapsulated sections. These losses are indicated in the photograph shown in Figure 4.7 which was taken with the bundle termination illuminated by an incoherent optical light source.

Figure 4.5. A Closeup Photograph of Test Panel A Showing the Optical Fiber Terminations and Details of the Stitching Pattern Employed to Attach the Cotton Backing to the Canvas Panel.

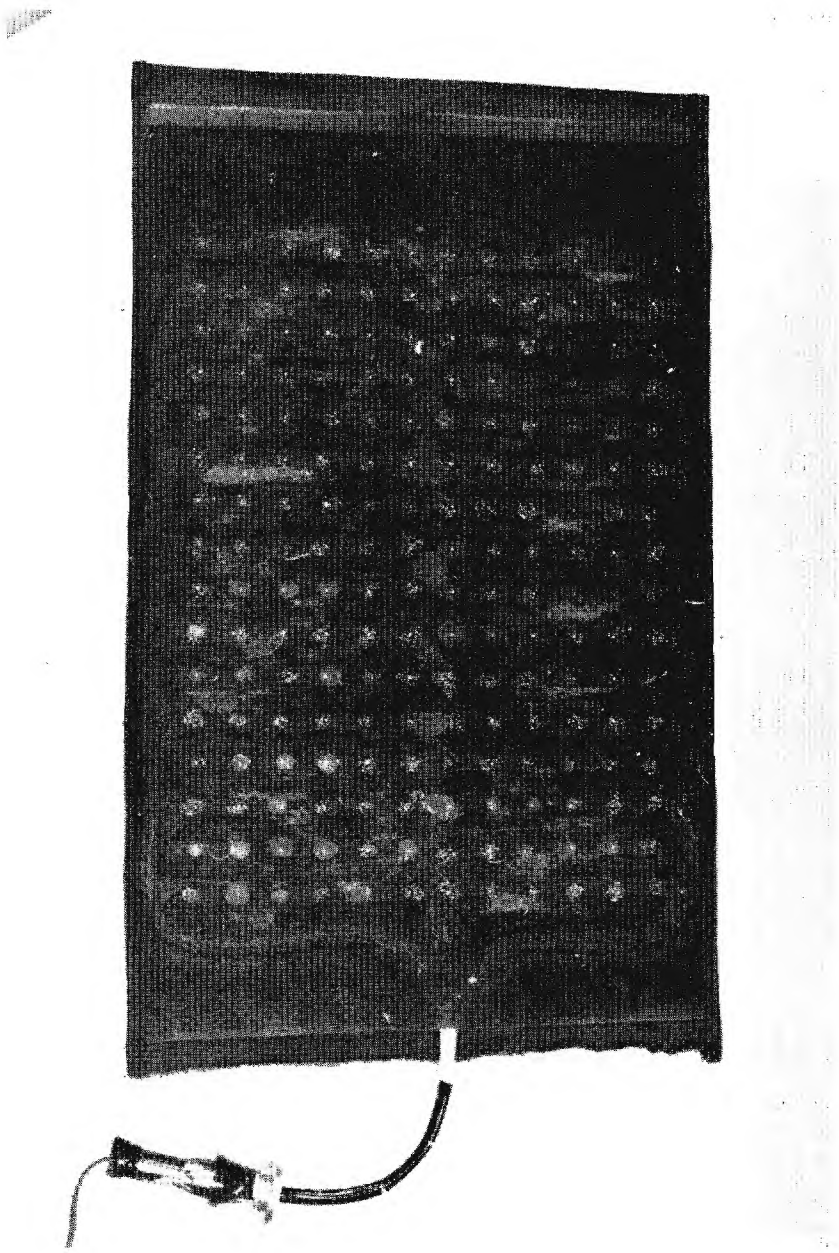

Figure 4.6. A Photograph of Test Panel A Showing the Fiber Bundle Termination and Test Optical Illuminator.

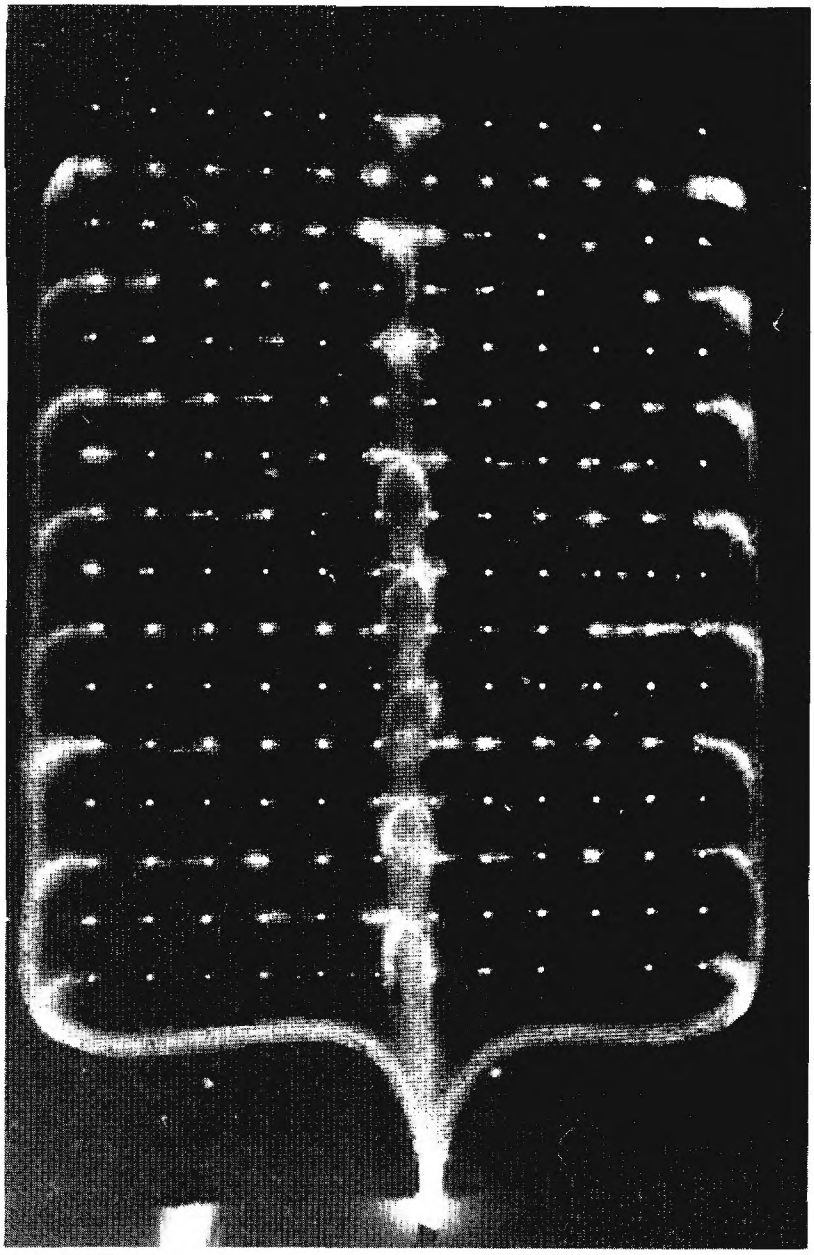

Figure 4.7. Photograph of Test Panel A Showing the Losses Incurred Along the Optical Fibers which were Imbedded in Epoxy and RTV Potting Compound.

Optical tests, which are described in Section 4.3.2, confirmed these observations indicating that the losses were higher than acceptable. Test samples were fabricated to determine why the bend losses were so much higher than had been previously measured. These measurements revealed that because the electromagnetic fields of waves propagating in fiber optic waveguides extend outside the cladding, when the fiber is bent encapsulated bends had significantly higher losses than did nonencapsulated bends. Additionally, for the same reason, losses along encapsulated straight sections were higher than along nonencapsulated sections. It was concluded from these measurements that the encapsulant significantly reduced the efficiency of the plastic fibers as light guides.

4.2.2 Modified Fiber Optic Detector Panel Design

With the results from the tests of Test Panel A and the supplementary results of the encapsulated samples, a modified detector panel (Test Panel B) was designed. Before the modified panel design was finalized, a number of test samples were fabricated, using the modified technique. Optical tests on these samples determined that coupling losses were comparable to those obtained for nonencapsulated fibers.

The second panel was fabricated using the same teflon fixture as with the first panel. The fabrication procecures, however, were modified as follows:

The fibers were first inserted through the teflon plate and through the vinyl-coated canvas. Rather than being pulled until most of the fiber was above the canvas as with the first panel, the fibers in the second panel were pulled only about 1 inch above the canvas. Once all the fibers were positioned, a fast-setting epoxy (Duro 5 Minute) was used to lock the optical fiber to the canvas. The epoxy was applied only along the straight section of the fiber at the point where the fiber passed through the canvas panel.

When the epoxy had set, the fiber ends immediately above the epoxy were cut with a new single-edge razor blade. The canvas with the fibers attached was carefully lifted from the teflon block, all fibers pulled completely through the teflon, and the assembly inverted.

The fibers were carefully bent over to parallel the canvas surface and laced into parallel rows running lengthwise the fabric. Figure 4.8 shows a cross-section of a fiber implant at this point. Once all the rows were laced into position, 1/3 x 1/8 inch polyurethane foam strips were bonded adjacent to and on each side of the rows of fiber optic fibers. Vinyl tubing 3/8 inch O.D. with 1/16 inch wall was cut lengthwise and positioned over each row of optical fibers and foam strips. The vinyl was tightly laced into position using multifilament polyester thread. A photograph of the partially completed Test Panel B in Figure 4.9 shows details of the fabrication technique described above.

The paralleled rows were then directed to a single gathering point approximately 1/3 the distance from the right side of the panel as viewed from the front. Multifilament polyester thread was used to lace the rows in the position described above. Figure 4.10 shows the panel at this stage of fabrication.

A medium weight cotton denim was then placed over the panel covering the vinyl strips. A multifilament thread was then used to machine sew the denim and detector assembly together. A seam was sewed between each row of fibers and around the perimeter of the panel. The collected fiber ends were all cut at the point where the shortest fiber ended. These ends were then potted into an aluminum fitting designed to mate with the photodetector assembly. Figure 4.11 is a photograph of the front surface of the completed panel.

Insertion loss measurements, which were described in Section 4.3.2, showed an improvement of 12.5dB for Test Panel B over Test Panel A. The photograph of Test Panel B with the fiber bundle end illuminated, which is shown in Figure 4.12, illustrates the remarkable improvement in light loss in comparison with the same test of Panel A which was shown in Figure 4.7. The uniformity of the array is demonstrated in Figure 4.13 which shows the light intensity pattern at the fiber bundle end resulting from illumination of the fiber optic array on Test Panel B. The illuminating source was a fluorescent lamp, and the lower intensity evident in several of the fiber ends is a result of the lamp's non-uniform intensity pattern since it was shown that the pattern of lower intensity fiber ends could be caused to change with small changes in the position of the lamp relative to the panel.

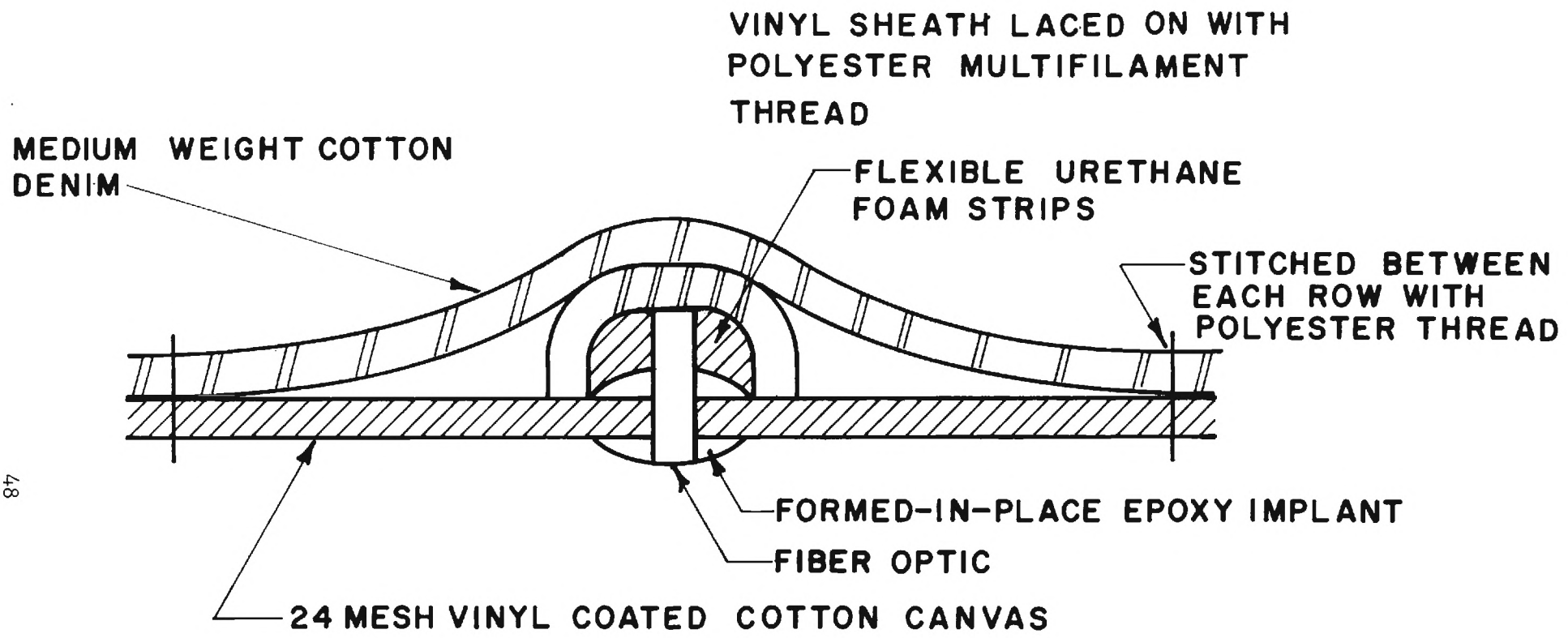

Figure 4.8. END CROSSECTION OF FIBER IMPLANT SHOWING PROTECTIVE STRIPS AND COVER

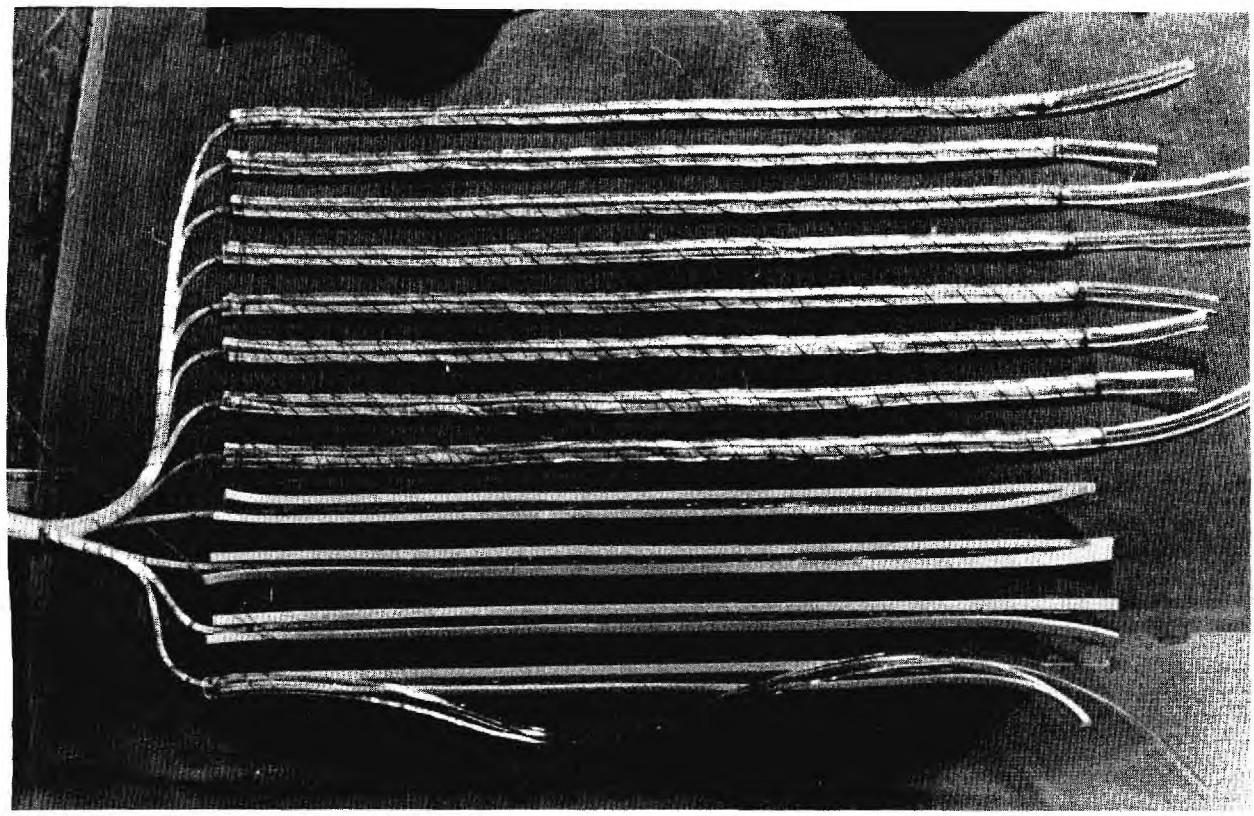

Figure 4.9. A Photograph Showing the Fabrication Technique Employed on Test Panel B.

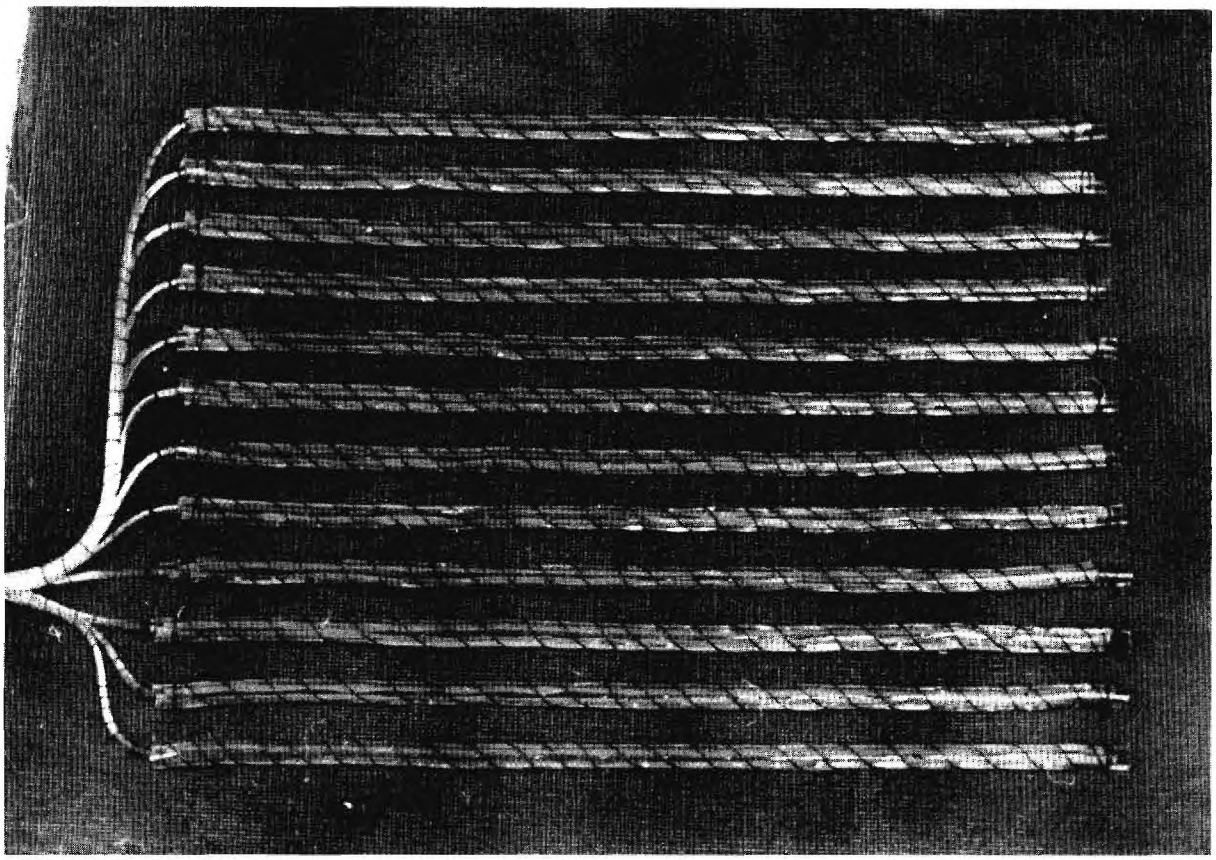

Figure 4.10. A Photograph of Test Panel B Prior to Attachment of the Cotton Backing Material.

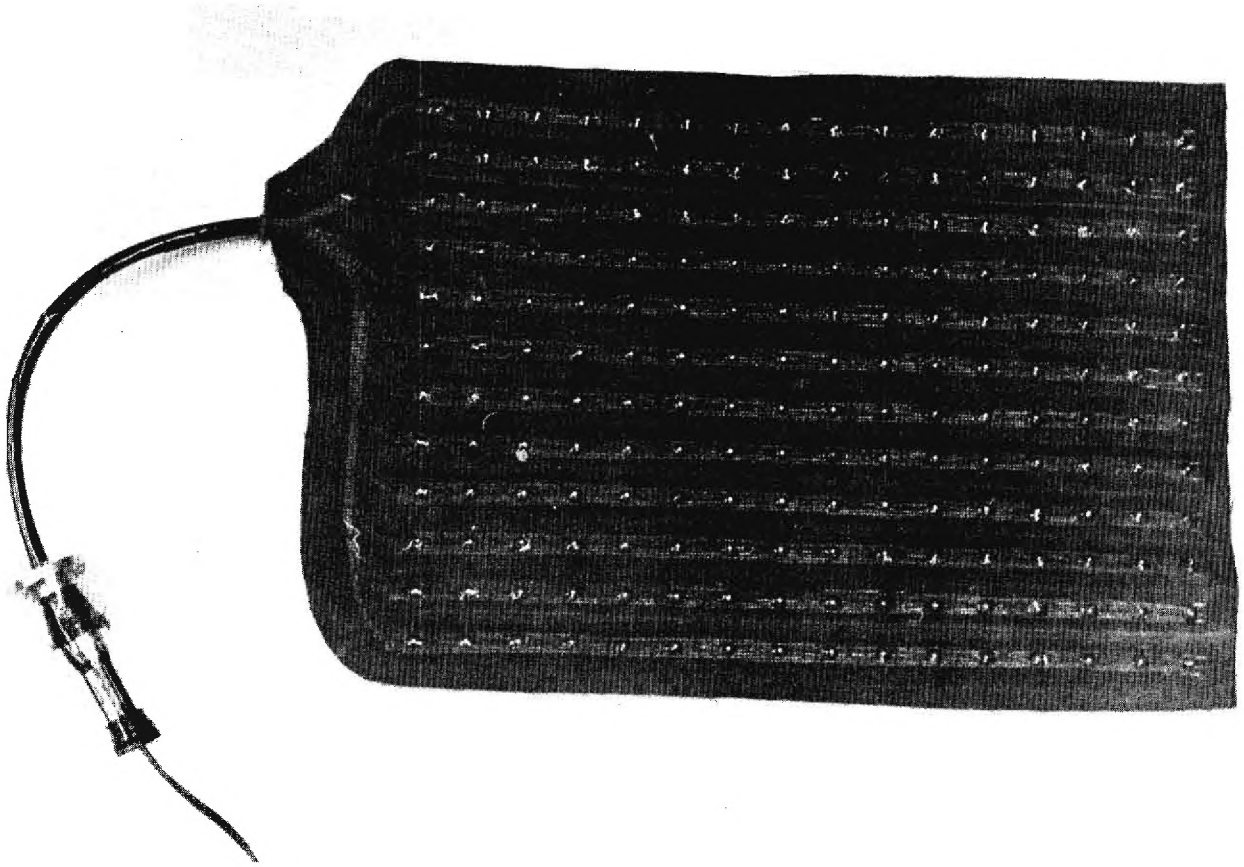

Figure 4.11. A Photograph of the Front Surface of Test Panel B.

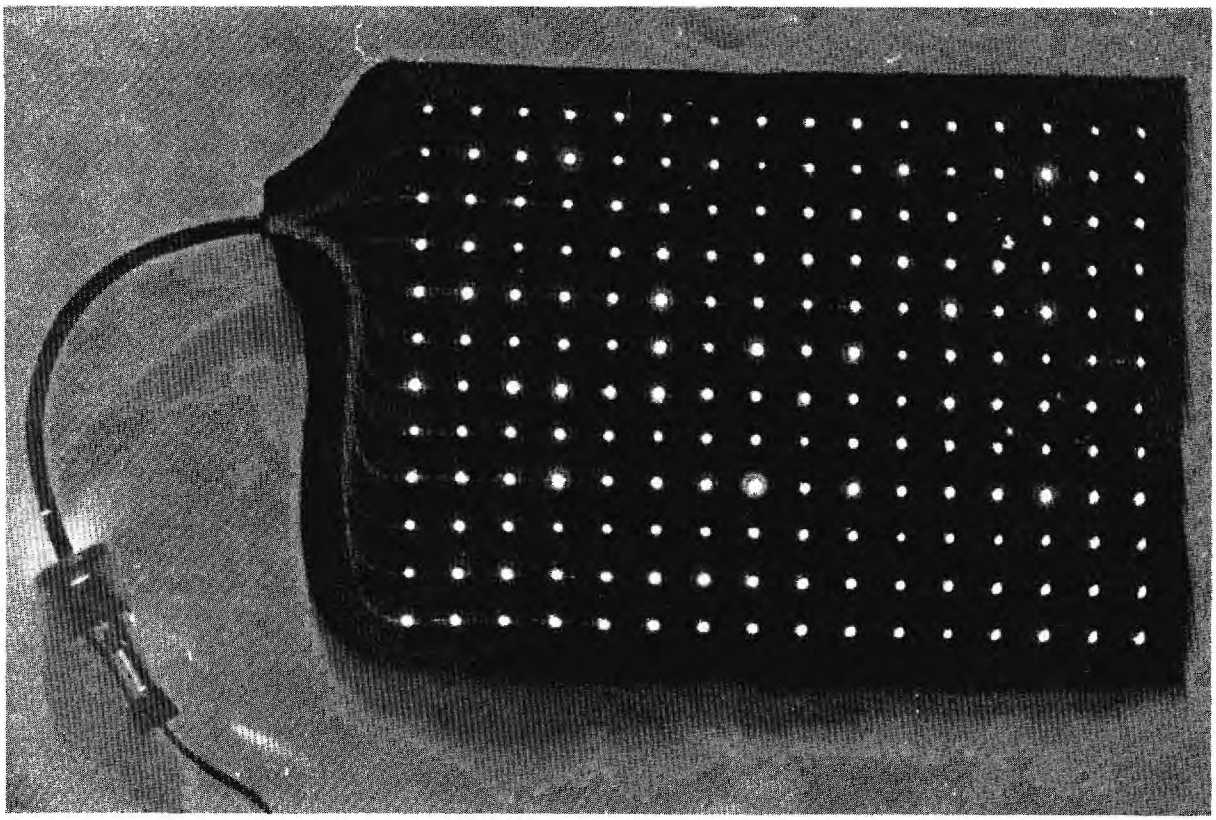

Figure 4.12. A Photograph of Test Panel B with the Fiber Bundle End Illuminated by an Incoherent Source.

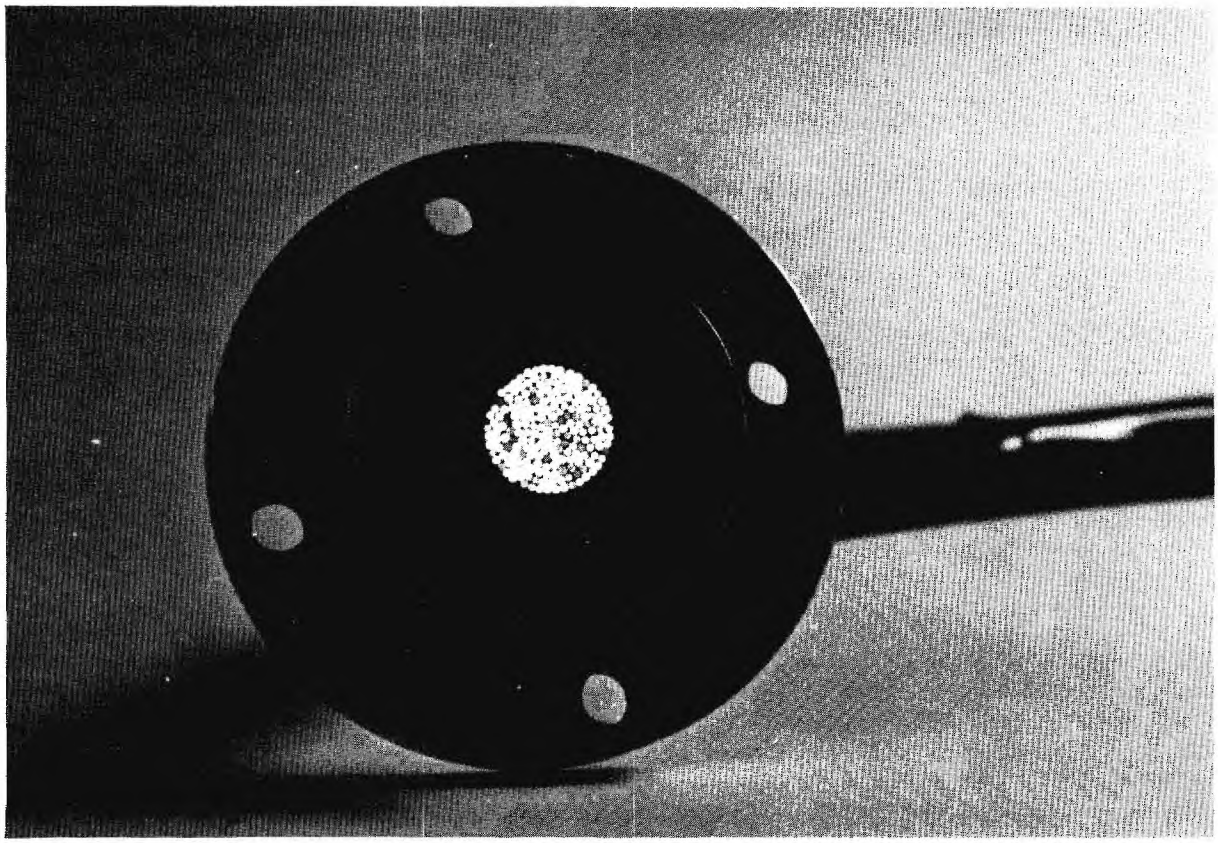

Figure 4.13. Light Intensity Pattern of the Fiber Bundle End Resulting from Illumination of Test Panel B with an Incoherent Light Source.

4.3 Detector Panel Optical Characteristics

4.3.1 Angle of Acceptance of the Panel

The angle of acceptance of the fiber optic panel was measured by mounting the panel on a rotating optical base and illuminating the panel with an incoherent light source which provided a uniform light flux over the active area of the panel. The rotating base was located on the optic axis of the illuminator in a configuration similar to that which was described in Section 3.1.3. The power output of the fiber bundle was measured as a function of angle of incidence of the illuminator beam for two panel orientations. For one orientation, the axis of rotation was parallel to the plane of the 90° fiber bend at the surface of the panel, and in the other orientation, the axis of rotation was perpendicular to the plane of the fiber bend.

Polar plots of the acceptance angle characteristics of both test panels for the two orientations described above are shown in Figures 4.14 to 4.17. For both panels, the acceptance angle for rotation about an axis parallel to the fiber bend plane is the same as that for the individual fiber, and the acceptance angle characteristic is distorted for both panels because of coupling in the fiber bend as rotation of the panel exposes the bend to the illuminator beam. Note that this effect is much greater in Panel A where the bends were potted in epoxy and the radiative losses were relatively large. This result is intuitively expected if reciprocity between the radiation and coupling mechanism of the fiber optic exists.

An effective detector for an individual soldier should provide hemispherical pattern coverage of the soldier's upper torso. It is evident from the acceptance angle data that this desired coverage can be achieved with careful selection of the location of detector panels which conform to the natural body contours.

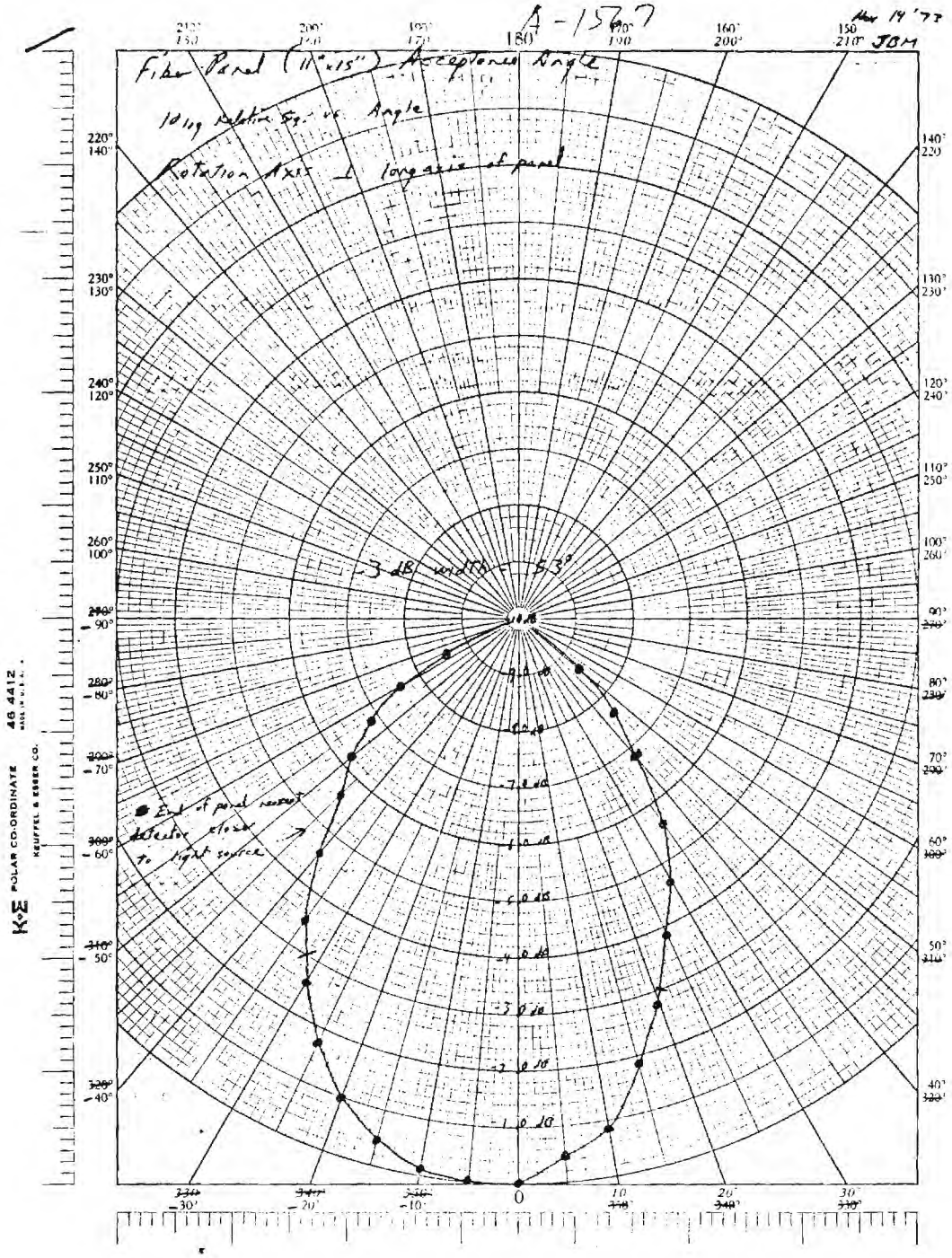

Figure 4.14. Acceptance Angle Characteristics of Test Panel A with Axis of Rotation Parallel to Fiber Bend Plane.

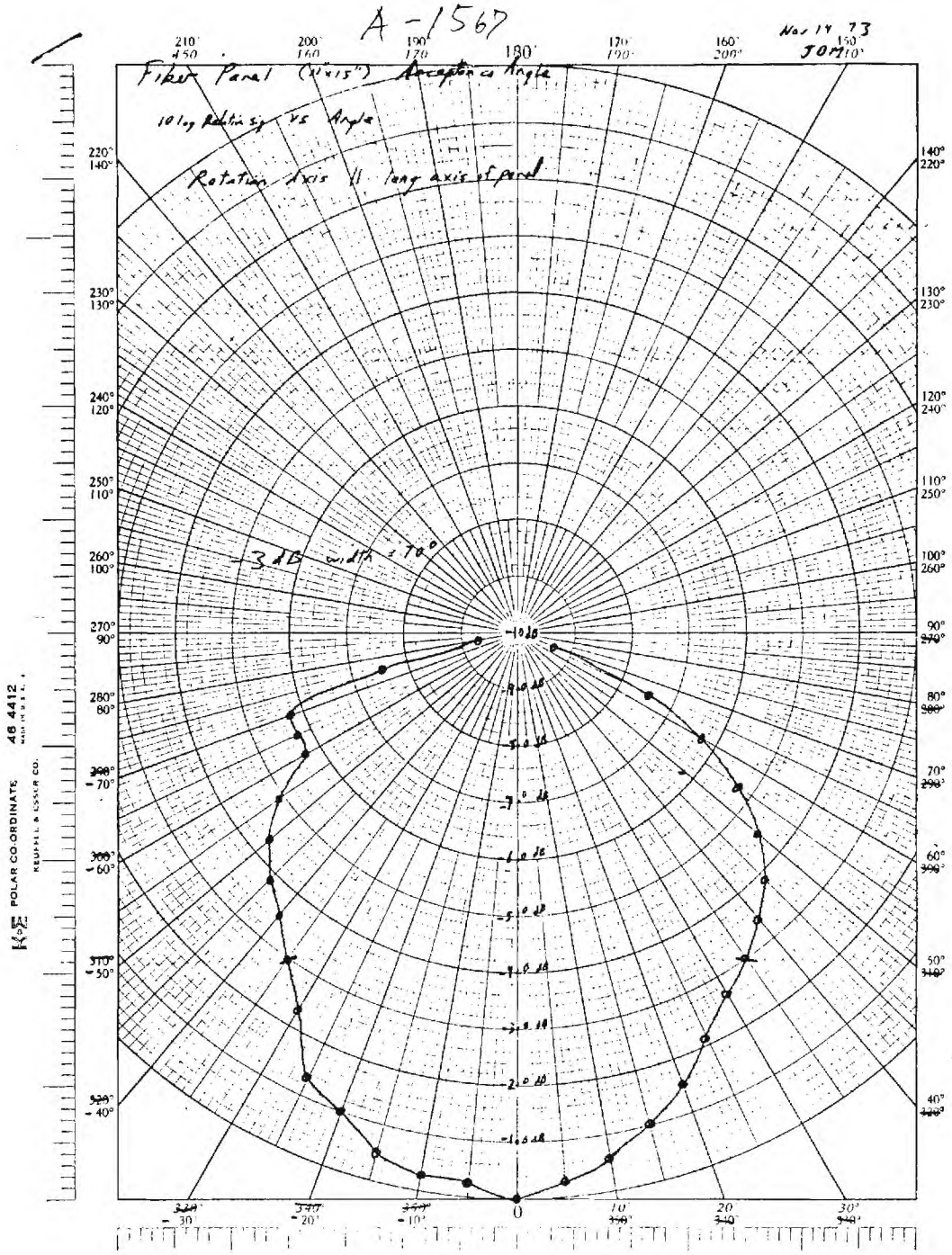

Figure 4.15. Acceptance Angle Characteristics of Test Panel A with Axis of Rotation Perpendicular to Fiber Bend Plane.

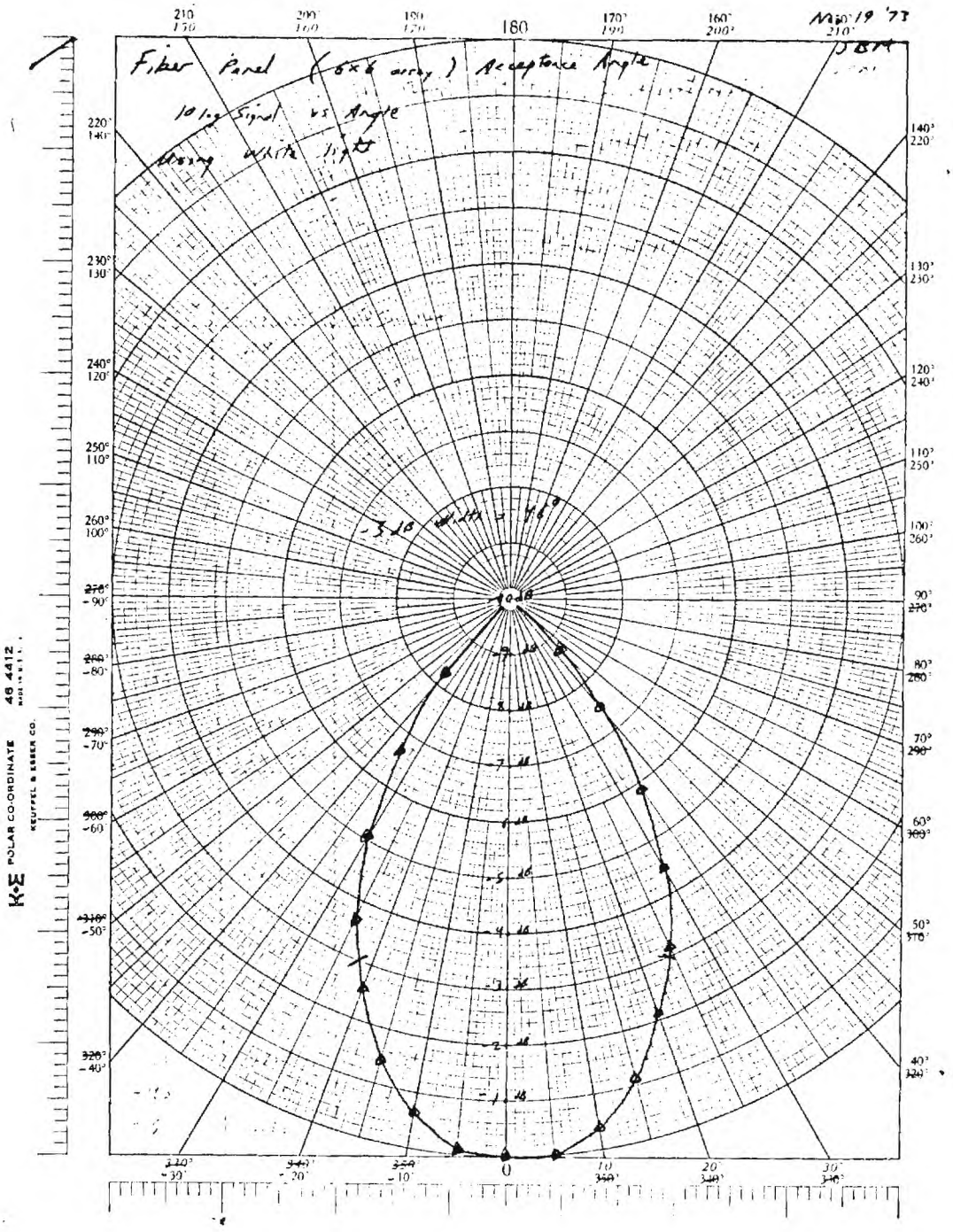

Figure 4.16. Acceptance Angle Characteristics of Test Panel B with Axis of Rotation Parallel to Fiber Bend Plane.

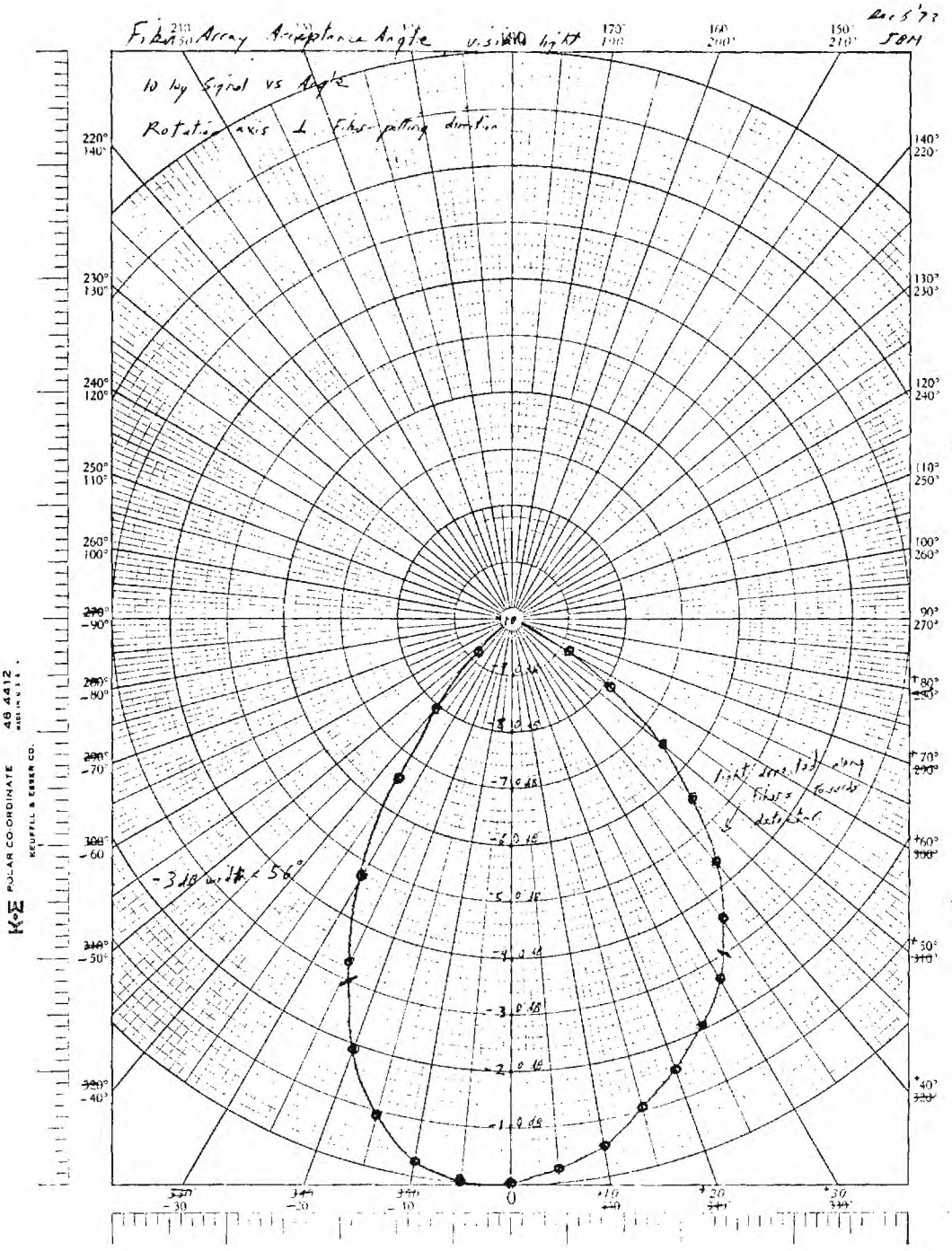

Figure 4.17. Acceptance Angle Characteristics of Test Panel B with Axis of Rotation Perpendicular to Fiber Bend Plane.

4.3.2 Insertion Loss of the Panel

The insertion loss of the panel was measured by illuminating the panel with a uniform light distribution and measuring the light emerging from the fiber optic bundle. This measurement yields an insertion loss parameter L_t which is composed of the following components:

a. Coupling loss from free space into the end of the fiber terminated in the panel (L_c)
b. Radiative loss in 90^o fiber optic bend at the back surface of the panel (L_b)
c. Absorption and scattering losses along the entire length of the optical fibers (L_a)
d. Coupling loss from the fiber end bundle termination into free space (Same as L_c)

The insertion loss parameter may thus be written as a function of its component parts:

$$L_t = L_a + L_b + 2L_c,$$

where the loss components are expressed in dB.

Experimentally, the insertion loss is determined by calculating the total power P_{tf} incident on all the fibers in the array from the measured light intensity. This calculation is performed from:

$$P_{tf} = I_{in} A_f N_f,$$

where I_{in} is the incident light intensity, A_f is the cross-sectional area of the fiber, and N_f is the number of fibers illuminated by the source. The insertion loss parameter, L_t is then calculated from:

$$L_t = 10 \log P_o/P_{tf},$$

where P_o is the power output of the fiber optic bundle end.

The incident light beam for these tests was derived from either a 60W tungsten lamp or a microscope illuminator, depending on the size of the target to be illuminated. The uniformity of the illumination was established by measurements utilizing the UDT Model 40A Radiometer detector as a probe. The average intensity of the 60W lamp was found to be $35 \mu W/cm^2$,

and the intensity was found to vary $< 1\mu W/cm^2$ over an 8 inch diameter area. Over an area of 12 x 15 inches, the average intensity was found to be $21\mu W/cm^2$ with variations $< 3\mu W/cm^2$. The microscope illuminator did not provide as good uniformity as the 60W bulb, but did provide a much higher intensity which proved useful in later tests. Its average intensity over a 12 x 15 inch area was found to be $340\mu W/cm^2$ with variations $< 60\mu W/cm^2$.

The efficiency, η, of the panel is defined by:

$$\eta = 10 \log P_c/P_{tp},$$

where P_{tp} is the total power incident on the panel. The relationship between the loss components - L_a, L_b and L_c and the total loss parameter L_t are discussed below.

Using the measurement technique described above, the insertion loss parameter, L_t, and the panel efficiency, η, were measured for Test Panels A and B, and for the 6 x 6 array panel developed earlier by EES. The results of these measurements are given in Table 4.1. The component losses based on these measurements and the previously measured fiber bend and absorption losses are presented in Table 4.2. The coupling loss component, L_c, is obtained by subtracting the measured component losses L_a and L_b from the measured panel insertion loss L_t and dividing by two. The small difference in the coupling loss so determined for Panels A and B, which both employ single, end-coupled fiber receptor points, provides a high level of confidence in the accuracy of the insertion loss measurements. The large difference in coupling loss between Panels A and B and the existing panel is a result of the uncertainty associated with calculating the cross-section of the multiple fiber receptors. Four of the five fiber ends are flared at the surface of the panel and hence present a reduced cross-section to the incident beam.

The significant improvement in insertion loss obtained by eliminating the epoxy and RTV potting compounds is evident. Additional improvements would require elimination of the 90° fiber bend or the development of a lower loss optical fiber with good mechanical properties. The configuration represented by Panel B is believed at present to be the best compromise between the optical and mechanical requirements associated with the subject application.

TABLE 4.1

INSERTION LOSS/EFFICIENCY OF THE END-COUPLED
FIBER OPTIC DETECTOR PANELS

Panel	L_t(dB)	η(dB)
A	21.7	56.5
B	9.2	43.5
Existing*	11.3	45.0

TABLE 4.2

LOSS COMPONENTS OF L_t FOR THE END-COUPLED
FIBER OPTIC DETECTOR PANELS

Panel	L_t(dB)	L_a(dB)	L_b(dB)	L_c(dB)
A	21.7	10.8	6.3	2.3
B	9.2	3.4	2.2	1.8
Existing*	11.3	4.2	0	3.6

*Multiple Fiber Receptors

4.3.3 Effects of Abrasion

The effects of abrasion were measured on samples of three different types of termination. The three terminations included the multiple fiber termination employed in fabrication of the existing target panel, the right angle termination employing the mirror, and the potted single bent fiber termination. In each case the measurement technique was the same. First, the power out of the fiber from the termination was measured. Then the face of the termination was abraided with sandpaper, and the power measured again. The loss (in dB) due to the surface roughness was calculated by

$$\text{Loss (dB)} = 10 \log \frac{P_o}{P}$$

where P_o = initial power output measured and

P = power output measured after the surface was roughened.

The termination consisting of five 10 mil Poly Optics fibers potted in an epoxy button showed a loss of 2.0dB due to surface roughness after sanding. The 45^o mirror, right-angle termination suffered a 2.1dB loss due to sanding. The lowest loss, 0.4dB, was shown by the bent fiber termination consisting of a single 20 mil Poly Optics fiber. Although these tests are difficult to relate to wear, which would be incurred in the intended application, it can be concluded that optically smooth surfaces are not required for operation of the detector panel, and that a relatively high degree of abrasion results in small losses.

5. ESTIMATED PERFORMANCE OF RECOMMENDED SYSTEM

5.1 Measured Signal-To-Noise Ratio

The end-coupled fiber optic array panel detector designated as Test Panel B in the discussion of Section 4.2.2 has been field tested at EMS and shown to be effective in scoring coded pulses from a collimated GaAs laser diode illuminator over the range of 25 to 300 meters. At the maximum range, the signal-to-noise ratio (S/N) for 95% detection probability was found to be 15dB. The field tests were, however, performed with an illuminator operating well below the eye safe intensity level for the pulse code format employed with the detector system.

5.2 Eye Safety Criteria

The eye safe illumination levels have been calculated from standards published by the Departments of the Army and Navy [5], ANSI [6], and have been confirmed in conversation with technical personnel at the Army Environmental Hygiene Agency [7].

The time-averaged intensity criterion for an eye-safe train of pulses from the diode laser can be calculated as follows:

$$\overline{\text{M.P.E.}} = L \times F \times R \times \text{M.P.E.}$$

where $\overline{\text{M.P.E.}}$ is the time averaged Maximum Permitted Exposure in W/cm^2.

- L is the wavelength correction factor, 2.5 for the diode laser wavelength of 0.9μm
- F is the pulse rate correction factor, 0.065 for a 437.2 Hz pulse rate
- R is the pulse rate
- M.P.E. is the Maximum Permitted Exposure per pulse, 5×10^{-7} Joules/cm^2/pulse for pulses of width in the range of 1 to 20,000 nsec.

Assuming a 437.2 Hz pulse rate, the $\overline{\text{M.P.E.}}$ is seen to be:

$$\overline{\text{M.P.E.}} = 2.5 \times 0.065 \times 437.2 \times 5 \times 10^{-7} \text{ W/cm}^2$$

$$\overline{\text{M.P.E.}} = 0.36 \times 10^{-4} \text{ W/cm}^2$$

$$= 36\mu\text{W/cm}^2$$

5.3 Calculated System Performance

Calculations were performed for the purpose of predicting the S/N for the illuminator-detector system, whose block diagram is shown in Figure 5.1. This block diagram represents the configuration of the system which was employed in the field tests. The power incident on the photodetector was calculated from measured system power levels and measured system component losses. The S/N was then estimated by comparing the calculated power level incident on the photodetector with the photodetector's noise equivalent power (NEP) in the electronic detector bandwidth.

The calculations were performed in accordance with equations (1) and (2)

$$P_o = P_i \eta T_F \tag{1}$$

$$\text{and} \qquad S/N = 10 \log \frac{P_o}{NEP}, \tag{2}$$

where P_o is the power incident on the photodetector, P_i is the power incident on the detector panel, η is the efficiency of the detector panel as defined in Section 4.3.2, and T_F is the transmissivity of the background radiation filter. P_i was determined from the beam spatial characteristics by employing a graphical technique for determining the total power contained within the intensity contours of the measured far field distribution. This power level was determined to be approximately 18 μW, which compares with the total power output of the illuminator aperture which was measured to be 29 μW. The difference of 2dB between these two values can be partially accounted for by atmospheric losses. For example, the molecular absorption by water vapor is approximately 1.5dB over a 300 meter path at 0.9 μm for 70°F and 50% relative humidity, and approximately 1.7dB for 70°F and 75% relative humidity. The beam spatial characteristics were measured at about 45°F and 50% relative humidity, and the loss for these conditions should fall approximately in the range above. Some of the apparent difference in the two power levels could be a result of error in the graphical technique employed in integrating the total power under the intensity contour plots.

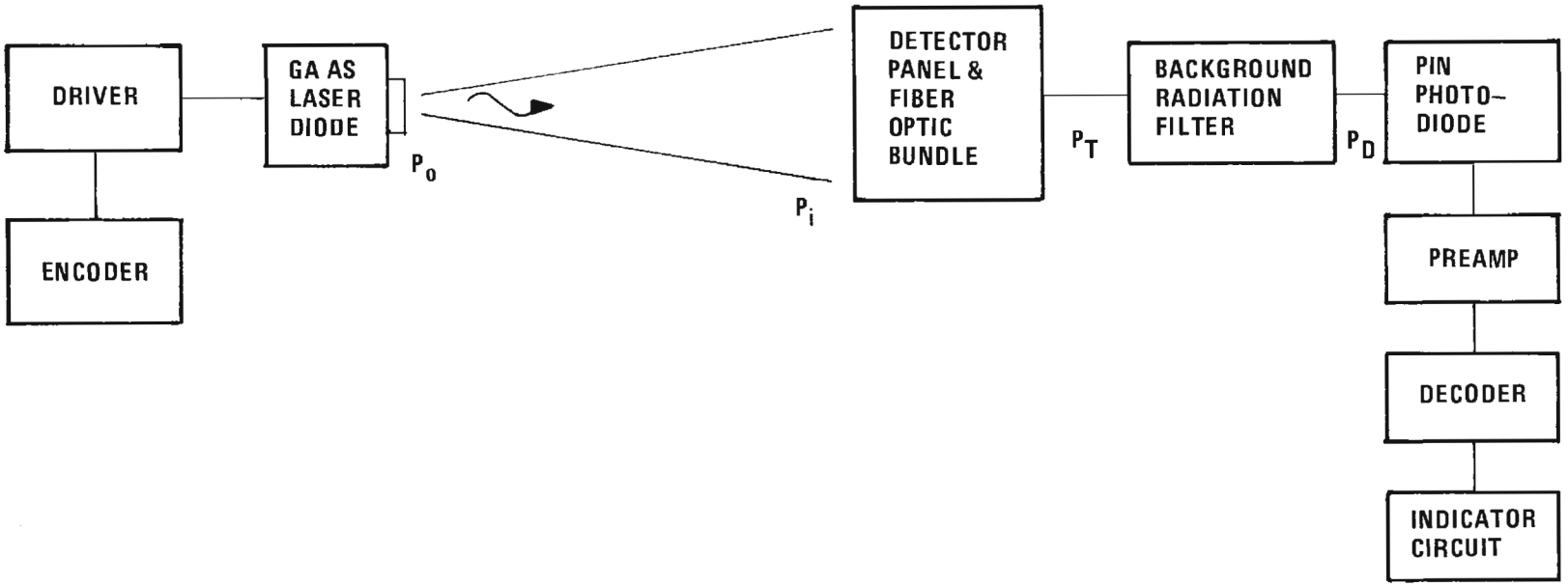

Figure 5.1. Block Diagram of the Laser Illuminator - Fiber Optic Array Detector System.

Thus the true value of P_i will be assumed to lie within the range 18-21 μW. The efficiency, η, of the detector panel was measured to be 4.47×10^{-5}, and the transmittance of the radiation filter was measured to be 0.82. From these values the power incident on the photodetector was calculated to fall within the range $6.6\text{-}7.7 \times 10^{-10}$ W.

From the published specifications on the RCA model C30809 photodetector, the NEP in a 40 kHz bandwidth (which is the approximate bandwidth of the detector electronics), is about 4.0×10^{-11} W, and comparing this value with those above for the power incident on the photodetector, the S/N was calculated to fall within the range 12.2 → 12.6dB. These calculations represent the maximum S/N which could be expected without pulse coding under ideal conditions. The field measurements have shown that the coded beam results in an increase of about 3dB in the system sensitivity. Thus the 3dB added to the calculated range of 12.2 → 12.6dB for the uncoded beam gives an estimated maximum S/N range of 15.2 → 15.6dB which is very close to the measured values.

5.4 Estimated Performance of an Optimized System

The measured intensity of the illuminator used in the field tests was $7.15\mu W/cm^2$ at the illuminator aperture. The eye safe level for the pulse code employed in the field tests was calculated above to be $36\mu W/cm^2$. Thus an improvement of 7 dB in S/N would be obtained from increasing the intensity to the M.P.E. level. There is also a degree of uncertainty concerning the collimation of the test illuminator. Although the far field radiation patterns indicate a beam spread of about 5.5 x 9.5 inches at 300 meters, the geometrical optics approximation for an incoherent extended source of the same dimensions as the laser diode and with the lens system employed in the illuminator would predict a beam spread of about 28 inches at 300 meters; however, this approximation should be applicable since the coherence between adjacent points along the diode's emitting junction is low. In addition, the intensity at 300 meters in a 5.5 x 9.5 inch beam area resulting from a 1 inch diameter illuminator emitting $7.15\mu W/cm^2$ should be about 108 nW/cm^2, whereas the measured average intensity is about 53 nW/cm^2.

Thus it would appear that allowing for atmospheric absorption of about 1.5dB, an additional increase of about 1.5dB could be expected from an illuminator with a smaller radiating junction resulting in improved beam collimation. Several techniques involving spatial filtering or optical waveguides could be employed to reduce the effective width of the diode's emitting region. Based on these considerations, it would appear that with an optimum illuminator configuration, a S/N of about 23dB could be obtained at 300 meters with Test Panel B.

Such a large S/N under optimum conditions would result in a system which would perform in more realistic training environments where losses might be incurred as a result of atmospheric scattering from rain, fog, dust and smoke, or reduction in detector panel cross-section caused by partial concealment, mud or other opaque materials partially covering the detector panel.

6. CONCLUSIONS AND RECOMMENDATIONS

6.1 End-Coupled Fiber Optic Detector Panel

The performance of the second panel fabricated under this program indicates performance well above panel requirements. Improvements in this type panel should be directed toward increasing the ease of fabrication. Several modifications look promising and should be investigated before proceeding to a production model.

6.1.1 Detector density should be decreased as much as possible while still maintaining adequate signal-to-noise ratio for conditions which will be encountered in realistic training exercises. Performance much greater than that required brings very few additional benefits and does result in additional cost and complexity due to the larger number of fiber optic array points involved.

6.1.2 The protective covering and strip padding employed along the optic channels should be a molded self-skinning urethane foam. This will decrease the number of components by a factor of two for each row of fibers, and result in a more flexible panel configuration.

6.1.3 A special open weave monofilament canvas should be woven to replace the vinyl covered cotton canvas used on the prototype. This will make fiber insertion easier and should open the way for ultrasonically sewed seams.

6.2 Side-Coupled Fiber Optic Detector Panel

A small 1.5 x 1.5 inch test sample was woven using the optic fibers as the weft and cotton fibers as the warp. A photograph of this sample is shown in Figure 6.1. Tests on this panel indicate that performance comparable to the 1 inch fiber optic end array should be possible. In this type construction, the light is coupled into the optical fibers from the side. At first glance this would appear to be much less efficient

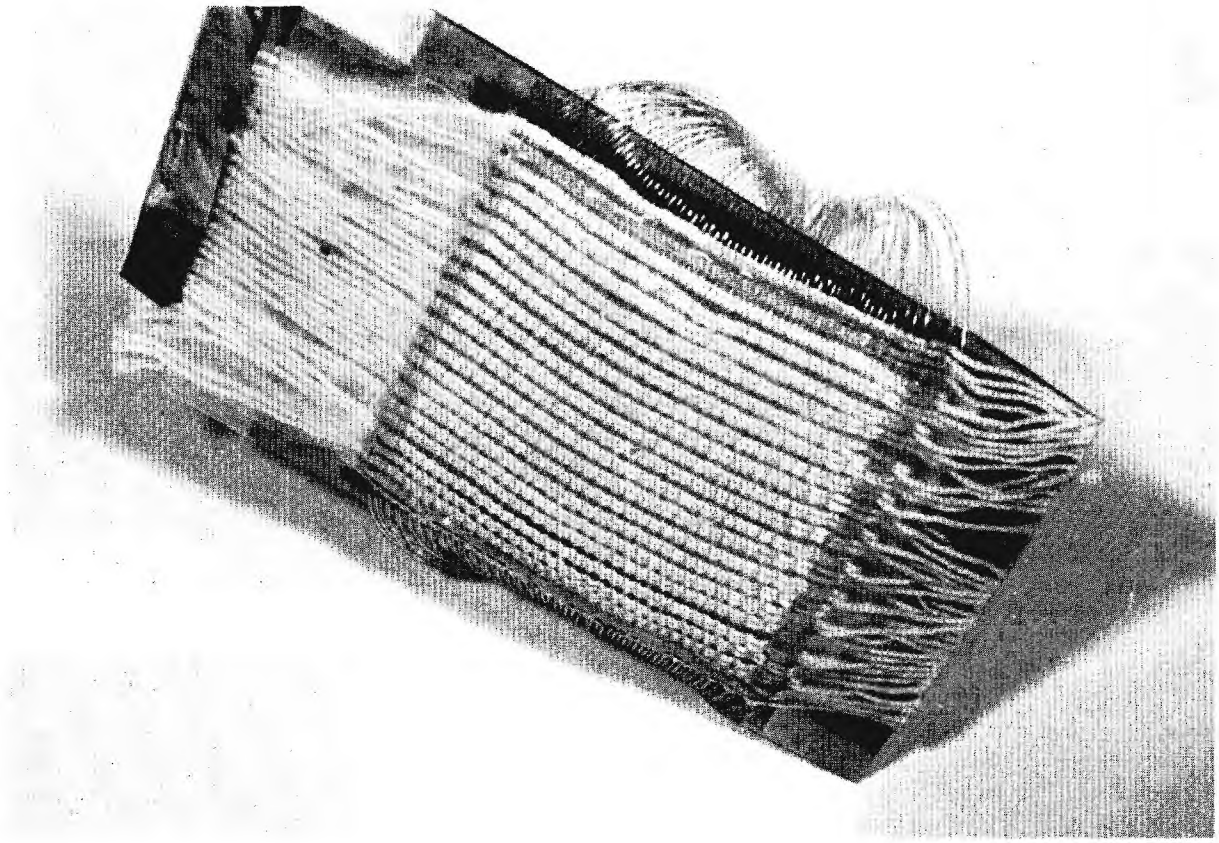

Figure 6.1. Photograph of the Woven Fiber Optic Test Sample.

due to the low side coupling efficiency which results from scattering in the fiber core. A closer look reveals that the area of optical fibers that is illuminated is so much larger in the woven construction that the poorer coupling efficiency is offset by the increased area. For example, the relative cross-section of the 1 inch end coupled array of 20 mil diameter fibers is about 3×10^{-4}, whereas the relative cross-section of the 1.5 x 1.5 inch test sample is about 0.1.

Cotton is certainly not the most desirable material to use when weaving a panel since it blocks the radiation where it loops over the optical fiber. It was used in the test sample because the warp on the loom was already cotton and required considerable work to change. Ideally the optical fibers should be used for the warp and a similar diameter clear monofilament fiber which is relatively transparent at 0.9μm wavelength be used as the weft.

For comparable optical performance, the woven construction has the following advantages over the implant construction:

1. Production costs should be made lower because, once the loom is set up, very little additional handling is required to complete a detector panel.

2. Panel thickness can be as thin as a single layer of cloth which is impossible with the implant technique. This feature would result in a more flexible panel which would also provide a greater number of options for integrating the panel into the soldier's standard clothing and equipment.

3. The woven construction offers redundancy to a degree not practical with the implant technique, i.e., loss of a single fiber would remove all detection capability in the one square inch area surrounding the fiber in the implant technique while losing as little as 1/20 of the detection capability in the same area in the woven technique.

4. The woven panel would also be more durable than the end array panel since the panel-fiber attachment points and the 90 degree fiber bends would be eliminated in the woven panel.

In view of the potential improvement associated with a woven fiber optic panel, it is recommended that the program be extended to permit setting up a small prototype loom with the optical fibers on the warp. This will permit evaluation of the effect of weft fiber diameter, stiffness, tension, color and other factors which might affect the coupling efficiency, and provide a direct comparison of the system performance of the two types of fiber optic array panels.

7. REFERENCES

1. "Technical Proposal Requirements for Laser Engagement System (LES) Devices 17A29-33," Naval Training Equipment Center, April 1973.

2. G.I.T. Proposal No. ST-STD-73-023 to EMS dated 16 April 1973 entitled "Development of an Experimental Laser Engagement System."

3. G.I.T. Proposal No. ST-STD-73-002 to EMS, Inc., dated 2 August 1972 entitled "Development of an Experimental Photodetecting Vest for a Laser Beam Rifle Scoring System."

4. Letter to EMS from EES dated 20 March 1973 stating restrictions applying to proprietary materials included in the referenced proposals and the subject Final Report.

5. "Control of Hazards to Health from Laser Radiation," Document TB MED 279, Departments of the Army and Navy, 24 February 1969.

6. "Standard for the Safe Use of Lasers," Document Z/136, American National Standards Institute, 29 February 1972.

7. Telephone Conversations with Mr. David Sliney at the Army Environmental Hygiene Agency, Edgewood Arsenal, Maryland.